



저작자표시-비영리-변경금지 2.0 대한민국

이용자는 아래의 조건을 따르는 경우에 한하여 자유롭게

- 이 저작물을 복제, 배포, 전송, 전시, 공연 및 방송할 수 있습니다.

다음과 같은 조건을 따라야 합니다:



저작자표시. 귀하는 원저작자를 표시하여야 합니다.



비영리. 귀하는 이 저작물을 영리 목적으로 이용할 수 없습니다.



변경금지. 귀하는 이 저작물을 개작, 변형 또는 가공할 수 없습니다.

- 귀하는, 이 저작물의 재이용이나 배포의 경우, 이 저작물에 적용된 이용허락조건을 명확하게 나타내어야 합니다.
- 저작권자로부터 별도의 허가를 받으면 이러한 조건들은 적용되지 않습니다.

저작권법에 따른 이용자의 권리는 위의 내용에 의하여 영향을 받지 않습니다.

이것은 [이용허락규약\(Legal Code\)](#)을 이해하기 쉽게 요약한 것입니다.

[Disclaimer](#)

Ph.D. THESIS

Section Loss Evaluation of Corroded Strands in
External Tendons of Bridges

교량 외부긴장재 부식 강연선의
단면손실 평가

2019년 2월

서울대학교 대학원

건설환경공학부

유 철 환

ABSTRACT

Section Loss Evaluation of Corroded Strands in External Tendons of Bridge

Chul-Hwan Yoo

Department of Civil and Environmental Engineering

Seoul National University

When prestressing tendons are corroded, a bridge owner must decide whether to replace or repair them. If this decision must be based on a destructive inspection method, section losses in the steel strands must be estimated by measuring either the corrosion depth or the perimeter of the corrosion area. For this study, corroded strands were sampled from a post-tensioned concrete box-girder bridge that demonstrated external tendon failure due to chloride- and moisture-induced corrosion to identify the characteristics of corrosion which occurred in field.

The corrosion characteristics of the corroded wires and strands were analyzed from the photograph taken from a cellphone with macro lens. It was identified that corrosion rapidly progressed along the perimeter in the earlier stages. The number of observable corroded wires and the visible characteristics such as corrosion depth and perimeter had a relationship with the section loss in strand.

Models for the determination of corrosion progress in corroded wires were investigated in a preliminary study of evaluating section losses in strands. Analysis showed that using models of existing corrosion progress routinely underestimated the section losses for corrosion depth. Actual measurements showed a corroded surface with a convex shape. New corrosion-models that more-accurately reflect

the actual corroded sections of wires are proposed. Although the measurements showed a large degree of dispersion, the proposed models were verified as more effective in estimating section losses.

Herein is described a process whereby section losses in corroded, seven-wire, strands can be accurately estimated via visual inspection. The cross-section of a strand is differentiated into visible and invisible regions. Corrosion is normally measured only in visible regions. This new process applies previously proposed geometric corrosion progress models for corroded wires to estimate section losses. The models were established to use corrosion depth and perimeter to estimate section loss of wires, and, therefore, both measurements were used to make estimations. Although the corrosion occurring in the invisible region cannot be measured directly, cross-section examinations have shown that corrosion in the invisible regions is minor. Compared with using the corrosion perimeter to estimate section losses, the use of corrosion depth is more accurate. The ultimate strength remaining in corroded strands was compared with estimates of section losses in order to confirm the applicability of the findings from this study. Mean corrosion depths of 5 and 15% or mean corrosion depth of 2% and 15% corresponded to ultimate strengths of 95 and 90%, respectively.

For reflecting the probabilistic characteristics of corrosion in strands, the Monte Carlo simulation was adopted. The various uncertainties contained in corroded strands were defined and constructed to statistical model. The simulation gives a number of corroded strands within a reasonable range. Based on the simulation result, the relationship between the section loss in strands and the corrosion depth or perimeter was established.

Keywords: Corrosion, Steel strand, Steel wire, External tendon

TABLE OF CONTENTS

1. INTRODUCTION	1
1.1 Research Background.....	1
1.2 Objective and scope	4
2. Measurement of the Cross Section of Corroded Wires and Strands	8
2.1 Sampling of Corroded Strands	9
2.2 Characteristics of Corroded Wires	12
2.2.1 Measurement of cross sections in corroded wires	12
2.2.2 Results of measurement	15
2.3 Characteristics of Corroded Strands.....	19
2.3.1 Measurement of cross sections in corroded strands	19
2.3.2 Visible and invisible region.....	20
2.3.3 Corrosion depth and perimeter in strand	23
2.3.4 Number of corroded outer wires	25
3. Modeling Corrosion Progress of Steel Wires in External Tendon	26
3.1 Corrosion Model of Wires using Corrosion Depth	27
3.1.1 Existing corrosion models	27
3.1.2 Proposed corrosion model I.....	31
3.2 Corrosion Model of Wires using the Corrosion Perimeter	35
3.2.1 Corrosion models with corrosion perimeter	36
3.2.2 Proposed corrosion model II	38
3.2.3 Limitation of Proposed model II	45
3.3 Corrosion Model of Wires using the Both Corrosion Depth and Corrosion Perimeter	50
4. Estimating Corrosion in the 7-wire Steel Strands of External Tendons.....	52
4.1 Using Corrosion depth to Estimate Section loss	53

4.1.1 Results of estimation	53
4.1.2 Analysis of Residuals – Section Loss Estimation Using Corrosion Depth	55
4.2 Using Corrosion Perimeter to Estimate Section Loss	61
4.2.1 Results of estimation	61
4.2.2 Analysis of Residuals – Section Loss Estimation Using Corrosion Perimeter	61
4.3 Using Both Corrosion Depth and Perimeter to Estimate Section Loss	65
4.3.1 Results of estimation	65
4.3.2 Analysis of Residuals – Section Loss Estimation Using Both Corrosion Depth and Perimeter	65
4.4 Evaluating the Remaining Strength of Corroded Strands	68
4.4.1 Strength degradation of corroded strands	68
4.4.2 Application of Section loss by Using Corrosion Depth for Ultimate Strength Evaluation	70
4.4.3 Application of Section loss by Using Corrosion Perimeter for Ultimate Strength Evaluation	72
5. Examining the Validity of the Estimation by Monte Carlo Simulation	75
5.1 Probabilistic Characteristics of Corrosion in Wires and Strands	76
5.1.1 Middle point of corrosion	76
5.1.2 Corrosion depth and perimeter by the location of middle point of corrosion	77
5.1.3 Probability distribution of corrosion depth and perimeter	78
5.1.4 Section loss in wires via corrosion depth and perimeter	82
5.2 Generation of Corroded Strands	88
5.2.1 Generation procedure	88
5.2.2 Generation of corroded wires and strands	90
5.2.3 Discussion of generated result	92
5.3 Application – Evaluating Remaining Strength of Corroded Strands	95
6. Conclusions and Recommendations for Future Study	97
REFERENCES	101

LIST OF FIGURES

Fig. 2.1 The post-tensioned segmental concrete box-girder bridge (SMFMC 2017): (a) typical view of outside box-girder ; and (b) typical view of inside box-girder	9
Fig. 2.2 Overview of the bridge: (a) side view; (b) section view; (c) close-up view of box A in (b); (d) cross-section of external tendon; and (e) cross-section of 7-wire steel strand	10
Fig. 2.3 Collected strands: (a) before cutting, (b) after cutting	13
Fig. 2.4 Photoshoot equipment: (a) assembly of macro lens and cell phone camera; and (b) photographing cut sections	14
Fig. 2.5 Measuring section loss due to corrosion: (a) original photo of corroded wire; and (b) identifying the corroded area	14
Fig. 2.6 Typical cross-sections of corroded wires: (a) section loss of 0% ~ 10%; (b) section loss of 10% ~ 20%; (c) section loss of 20% ~ 30%; (d) section loss of 30% ~ 40%; (e) section loss of 40% ~ 50%; and (f) section loss of 53%	15
Fig. 2.7 Measuring corrosion properties: (a) corrosion perimeter; and.....	16
Fig. 2.8 Variations in corrosion shape with respect to section loss:	18
Fig. 2.9 Cross-section of a corroded strand: (a) photograph of a corroded strand section; and (b) identified cross-section	20
Fig. 2.10 Identifying visible and invisible regions in the cross-section of a corroded strand	21
Fig. 2.11 Cross-sections of strands corroded in the invisible region: (a) section loss of 1.1%; (b) section loss of 1.3%; (c) section loss of 2.0%; (d) section loss of	

7.7%; and, (e) section loss of 16.8%	22
Fig. 2.12 Section losses of corroded strands with respect to the following: (a) mean corrosion depth in the visible region; and (b) mean corrosion perimeter in the visible region.....	24
Fig. 2.13 Section losses of corroded strands with respect to the number of corroded outer wires identified in the visible region	25
Fig. 3.1 Configuration of idealized corrosion: (a) Val and Melchers' model (1999); and (b) Hartt and Lee's Model (2016).....	28
Fig. 3.2 Comparison between measured corroded wire sections and corrosion models: (a) section loss versus corrosion depth; and (b) zoom in of box A.....	30
Fig. 3.3 Configuration of Proposed corrosion model I.....	32
Fig. 3.4 Comparing residuals of section loss for each model: (a) Val and Melchers' model; (b) Hartt and Lee's model; (c) Proposed model I; and (d) Proposed model II	34
Fig. 3.5 Comparison between measured corroded wire sections and corrosion models: (a) section loss versus corrosion perimeter; and (b) enlargement of box A	37
Fig. 3.6 Regression analysis results between averaged corrosion depth and corrosion perimeter	39
Fig. 3.7 Configuration of Proposed corrosion model II	42
Fig. 3.8 Comparing residuals of section loss for each model: (a) Val and Melchers' model; (b) Hartt and Lee's model; (c) Proposed model I; and (d) Proposed model II	43
Fig. 3.9 Comparing cross-sections of each model and measured section for the section losses of 10%, 30% and 50%: (a) 10% section loss of Val and	

Melchers' model; (b) 30% section loss of Val and Melchers' model; (c) 50% section loss of Val and Melchers' model; (d) 10% section loss of Hartt and Lee's model; (e) 30% section loss of Hartt and Lee's model; (f) 50% section loss of Hartt and Lee's model; (g) 10% section loss of Proposed model I; (h) 30% section loss of Proposed model I; (i) 50% section loss of Proposed model I; (j) 10% section loss of Proposed model II; (k) 30% section loss of Proposed model II; (l) 50% section loss of Proposed model II; (m) 10% section loss of a typical measured section; (n) 30% section loss of a typical measured section; and (o) 50% section loss of a typical measured section	44
Fig. 3.10 Corrosion depth and perimeter of wires in strand by the target range	47
Fig. 3.11 Value of cross-validation by degree of polynomial.....	47
Fig. 3.12 Result of regression with newly determined target range.....	48
Fig. 3.13 Comparison between measured corroded wire sections and corrosion models: (a) versus corrosion depth; (b) versus corrosion perimeter.....	49
Fig. 3.14 Comparison between measured corroded wire sections and corrosion models: (a) section loss versus the product of corrosion depth and corrosion perimeter; and (b) plotting in log scale.	51
Fig. 4.1 Comparison of actual and estimated section losses for corrosion depth: (a) estimated in visible region; and (b) estimated in whole region.....	54
Fig. 4.2 Residuals of section loss: (a) caused by the corrosion model; (b) caused by limited visibility; and (c) total residuals.....	57
Fig. 4.3 Cross-section <i>a</i> in Fig. 4.1 and Fig. 4.2	59
Fig. 4.4 Cross-section <i>c</i> in Fig. 4.1 and Fig. 4.2.....	60
Fig. 4.5 Comparison between actual and estimated section losses for a corrosion perimeter: (a) estimated in the visible region; and (b) estimated in an entire	

region.....	63
Fig. 4.6 Residuals of section loss: (a) caused by wire model; (b) caused by visual limit; and (c) total residuals.....	64
Fig. 4.7 Comparison between actual and estimated section losses for the product of corrosion depth and perimeter: (a) estimated in the visible region; and (b) estimated in an entire region	66
Fig. 4.8 Residuals of section loss: (a) caused by wire model; (b) caused by visual limit; and (c) total residuals.....	67
Fig. 4.9 Results of tensile test in Jeon et al. (2017).....	69
Fig. 4.10 Evaluating the remaining ultimate strength of corroded strands using estimates of section losses.....	71
Fig. 4.11 Results of regression analysis: (a) comparison of actual and estimated section losses in visible region; (b) evaluating the remaining ultimate strength of corroded strands using estimates of section losses.	73
Fig. 5.1 Middle point of corrosion	76
Fig. 5.2 Value of cross-validation by degree of polynomial: (a) corrosion depth; and (b) corrosion perimeter.....	86
Fig. 5.3 The results of GLM: (a) for corrosion depth; and.....	87
Fig. 5.4 Flowchart of generating the corroded strands.....	89
Fig. 5.5 Results of generation in terms of wires: (a) corrosion depth;	90
Fig. 5.6 Results of generation in terms of strands	91
Fig. 5.7 Regression analysis for measured strand cross section with respect to mean corrosion perimeter: (a) considering all of wires; and (b) excluding wires which have an asymptomatic corrosion.	93
Fig. 5.8 Regression analysis for measured strand cross section with respect to mean	

corrosion perimeter: (a) considering all of wires; and (b) excluding wires
which have an asymptomatic corrosion.94

Fig. 5.9 Remaining strength of generated strands: (a) vial mean corrosion depth;.96

LIST OF TABLES

Table 2.1 Section Losses in Each of the Wires Presented in Fig. 2.10.....	21
Table 4.1 Ranges of Ultimate Strength of Corroded Strands and Corresponding Mean Corrosion Depth	71
Table 4.2 Ranges of Ultimate Strength of Corroded Strands and Corresponding Mean Corrosion Perimeter	74
Table 5.1 Frequencies of the middle point of corrosion	77
Table 5.2 The mean and standard deviation of corrosion depth and perimeter by the angle of the middle point of corrosion	78
Table 5.3 Probability density function of examined probability distributions	80
Table 5.4 The most suitable distribution obtained from K-S test, AIC and BIC via corrosion depth.....	81
Table 5.5 The most suitable distribution obtained from K-S test, AIC and BIC via corrosion perimeter	81
Table 5.6 Parameter of Rayleigh distribution via corrosion depth and perimeter for each interval	82
Table 5.7 Common link functions	84
Table 5.8 Rank of goodness of fit as a distribution of the section loss in wire	85
Table 5.9 Canonical link function for each exponential families	85
Table 5.10 Regression coefficient obtained from GLM	86
Table 5.11 Number of strands sorted by number of corroded outer wires	88

CHAPTER 1

INTRODUCTION

1.1 Research Background

Prestressing tendons are composed of ducts, filling material, and groups of steel strands. The steel strands provide resistance to loads, and the duct and filling materials protect the steel strands from contaminants. Therefore, any defect in the duct or the filling material could cause damage to the steel strands and eventually threaten the safety of a bridge. Damage to steel strands could be in the form of corrosion or cracks. In particular, corrosion is the major type of damage that occurs (Kilduff et al. 2013).

When the section loss in corroded steel strands passes a certain level, a fracture in the prestressing tendon could occur (Hartt and Lee 2016; Trejo et al. 2009). In 1967, the Bickton Meadows Bridge in the United Kingdom (U.K.) collapsed (Poston and Wouters 1998). That collapse was the first recorded failure of a segmental post-tensioned bridge due to corrosion in prestressing tendons. Water with high chloride content infiltrated the tendon at the joints of the segments and caused corrosion in the steel strands. By the year 1985, two more segmental post-tensioned bridges had collapsed in U.K. During this period, several segmental post-tensioned bridges were inspected, and severe corrosion was found in tendons. The major reasons for the corrosion in these bridges were infiltration of chloride and moisture from concrete spalling and gaps between segments. These bridges were either reconstructed, or the tendons were replaced. In 1992, the Department of Transportation in the U.K. placed a moratorium on grouted tendons and inspected all existing

post-tensioned bridges over a period of five years (fib 2001). In these inspections, examples of voids in the grout and tendon corrosion were found in 53% and 52% of 447 bridges, respectively. In Austria, inspection of prestressing tendons was performed for ten post-tensioned bridges constructed between 1956 and 1973 (Eichinger et al. 2000). Endoscopy was used to inspect 10,188 spots in the tendons. Moderate and removable corrosion was found in 2% and 30% of inspected spots, respectively. Similar inspection was performed for the Omi Bridge in Japan (Nakagawa and Mikami 2010). Corrosion in strands was found in 27% of 544 inspected spots. Corrosion in prestressing tendons has also been detected in bridges in the United States (Hartt and Venugopalan 2002; Permeh et al. 2016; Trejo et al. 2009). Since 1999, corrosion in strands was detected in several segmental post-tensioned bridges in the states of Florida, Texas, Virginia, and Minnesota. Investigation revealed that the corrosion was caused by the infiltration of chloride and moisture into the tendons, high chloride or sulfate content in the grout, and the generation of corrosion currents between dissimilar types of grout following retrofitting. These examples demonstrate that corrosion in prestressing tendons is an inherent defect and is difficult to avoid.

Corrosion in a strand reduces not only the size of its cross-section, but also its load-carrying capacity (Betti et al. 2005; Nakamura and Suzumura 2012). In this reason, detecting corrosion at an early stage and evaluating the section loss of strand are critical to cope with corrosion because corrosion in strands is progressive until it is repaired. Since strands are protected by duct and filling material, both destructive and non-destructive methods are used to detect corrosion damage in tendons.

Non-destructive methods have the advantage of not opening the ducts by indi-

rectly detecting damage to the tendons. Damage can be detected by using a magnetic field, ultrasonic waves, radiography, or elastic impulses. Recently, Jones et al. (2010) conducted blind testing for six types of non-destructive methods and evaluated their accuracy and reliability for detecting corrosion. They found that the Magnetic Flux Leakage and Remnant Magnetism methods are potentially viable for detecting non-visible corrosion in prestressing strands. When similar testing was conducted by the Seoul Metropolitan Facilities Management Corporation (SMFMC) in the Republic of Korea, however, those methods were unsatisfactory (SMFMC 2017). Accuracy was highly dependent on the capabilities of the operator, and the size of the device limited the applicability of those methods. Therefore, non-destructive methods continue to be useful and needed, but improvement is required.

Destructive methods make it possible to directly observe strands and their surrounding environment such as the existence of voids, traces of bleeding or water leakage, or the quality of grout (Azizinamini and Gull 2012; Trejo et al. 2009). Observation can be performed via the naked eye or by using either an endoscope or a borescope after opening the duct. Sounding inspections via the use of a steel-tapping hammer are normally conducted prior to the opening of a duct. Tapping can reveal voids in the tendons via the detection of high pitches and irregular sounds. Destructive methods can easily confirm the existence of corrosion, but it is difficult to quantify a section loss in strands, which is directly related to the tensile strength of the tendons.

As a measure against this unquantifiable problem of section loss, Berg and Schokker (2012) applied the visual standard suggested by Sason (1992), which was adopted in PTI (2012) as an acceptance criteria for the installation of corroded

strands in the ducts, to evaluate corroded strands of Plymouth Avenue Bridge in Minnesota. The visual standard categorized strands by corrosion appearance. Moreover, Reis (2007) conducted tensile test for strands in San Francisco-Oakland Bay Bridge and found that the strands which could not satisfy the acceptance criteria according to the visual standard could not pass one of the minimum requirement for the ultimate strength or elongation or both. Since the visual strand only gives a qualitative evaluation of corroded strand, the quantifiable evaluation of section loss in strand still remains a problem.

1.2 Objective and scope

In 2016, external tendon failure occurred in one of the post-tensioned segmental concrete box girder bridges in Seoul, Republic of Korea. After the accident, a research project investigated the cause of the tendon failure and prepared a plan to repair and retrofit damaged tendons, as well as establishing a maintenance plan. As part of this research, tensile testing was conducted to verify the tensile strength of the corroded strands (Jeon et al. 2017). Test results showed that the reduction in tensile strength was greater than the section loss. This observation was also supported in a study by Betti et al. (2005). To decide whether corroded tendons should be repaired or replaced, the remaining strength of the corroded strands must be evaluated. Since the strength is dependent on the remaining sections in the strand, section loss in the strands must be determined. As mentioned earlier, the accuracy and reliability of non-destructive methods is questionable so that an evaluation method to estimate section loss in strands by destructive methods is required.

As a first step to estimate the section loss in strands, the cross sections of corroded strands which collected from near the failure location are investigated to

identify the characteristics of corrosion which occurred in field. The section loss in strands can be measured by several ways. The frequently used method is measuring average section loss by measuring the weight change before and after corrosion (ASTM. 1999; Lee et al. 2017; Wu and Li 2016). The corrosion depth is also measured frequently by either a micrometer or a pit depth gauge instead of section loss (ASTM. 2005; Gonzalez et al. 1995). Li et al. (2017) modeled corroded cross-section by measuring depth, width and length of corrosion pit using Vernier caliper. These approaches tried to find the section where corrosion was most severe instead of average section loss, but the actual section was not specifically measured. To identify the actual section loss, the measurement of corroded strands is performed by a photograph taken by the cell phone camera with macro lens in chapter 2. Based on the photographs, the section loss, the corrosion perimeter and the corrosion depth in wire and strand are identified. The focus of this investigation is limited to the cross section of corroded strands which is directly related to the strength of strands.

To estimate the section loss in wire by the length parameter such as corrosion depth or corrosion perimeter, the corrosion model which reflects the characteristics of corroded wires is investigated in chapter 3. The corrosion model is tasked with idealizing the configuration of the corroded section of a wire, because measuring the section loss in wires is a challenge while a bridge remains in service. If a corroded wire could be measured for pit depth or corrosion surface area, the model could then be used to estimate the section loss in the wire. Two corrosion models have been proposed by Val and Melchers (1997) and Hartt and Lee (2016). Val and Melchers assessed the time-variant reliability of deteriorating reinforced concrete slab bridges by assuming pitting corrosion in the rebar. This model has been widely

adopted to simulate pitting corrosion in rebar (Berto et al. 2009; Hackl and Kohler 2016; Kim et al. 2013; Stewart and Rosowsky 1998) and in wire (Darmawan and Stewart 2007; Guo et al. 2010). Hartt and Lee's model assumed the corroded surface of a wire would be flat while the corrosion is in progress. They used this model to assess the probability of failure for wires, strands and tendons. However, these existing models were not verified by comparing the measured cross sections of wires. Before establishing a corrosion model, the section configurations of corroded wires in field should be analyzed. Based on the observation result of corroded wires in field, new corrosion models are proposed for corrosion depth and perimeter, respectively. The applicability of these models should be evaluated by comparing the corroded sections of wires. The examined wires are not procured by accelerated corrosion testing but are collected from a bridge with corroded tendons that had failed.

The advantage of these models is that the inspector could estimate the section loss in wire by measuring the corrosion depth or the corrosion perimeter. However, it is desirable to estimate the section loss in strand instead of the section loss in wire for the practical purpose. Unlike a wire, the inspector cannot investigate the whole of strand because of the geometric properties of strand. Moreover, there are many obstacles in field to inspect an whole strand such as grout residue, the arrangement of strand in tendon. In this respect, this thesis assumes that an entire strand can be observable. The usable information for estimating the section loss in strand is the corrosion state of entire strand identified from the endoscope or the visual inspection. Therefore, the model which estimates the section loss in strand is proposed with the limited information in chapter 4 as an extension of proposed wire model. In this regard, this model can provide an initial stage and the primary

way to evaluate the section loss in strand which experiences the corrosion damage.

Chapter 4 provides the model for estimating the section loss in strands by deterministic approach. However, the section losses in wire and strand include the uncertainty for the corrosion depth and perimeter. In this regard, the section loss should be treated by a probabilistic tool. In this purpose, chapter 5 accesses the estimation of section loss in strand by probabilistic approach. The Monte Carlo simulation (MCS) is adopted to manage the various combination of corrosion. Before conducting MCS, the probabilistic characteristics of corrosion in wires and strands should be established. Probabilistic parameters considered in this thesis contain the location of corrosion, the characteristics of corrosion depth and perimeter by the location of corrosion, the variability of section loss in wire and the number of corroded outer wires.

The estimation of section loss in strand should be examined in terms of strength because the degraded strength of corroded strand is a main concern to decide whether corroded tendons should be repaired or replaced. For this examination, the example of applying the estimation method is introduced in terms of strength of corroded strand. Through this example, the applicability of the estimation is examined.

CHAPTER 2

Measurement of the Cross Section of Corroded Wires and Strands

Most of studies (Kashani et al. 2013; Li et al. 2014; Provan and Rodriguez III 1989; Stewart 2004) conducted an corrosion acceleration test for obtaining the corroded samples. The advantage of corrosion acceleration test is spending a short time for inducing corrosion by exposing to the extremely corrosive environment. Even if this corrosive environment in laboratory may simulate the extremely corrosive condition of actual environment, it is not verified that the characteristics of corrosion induced in laboratory will be same with the corrosion occurred in actual situation. In this respect, the best way to identify the characteristics of corrosion in actual condition will be collecting the samples from the operating bridge site.

In this study, the corroded samples were collected from the operating bridge site. Although the exact corrosive conditions of collected strands such as chloride content, water and cement ratio of grout were not identified, the collected samples will be useful to understand the characteristics of corrosion in actual condition. The collected samples are analyzed with respect to the wire and the strand for identifying the corrosion characteristics in both wire and strand level.

2.1 Sampling of Corroded Strands

The failure of tendons occurred in a post-tensioned segmental concrete box-girder bridge (see Fig. 2.1), which has been in place since 1999, due to a corrosion at 2016 in Seoul, Republic of Korea. The failure was found in one of the external tendons above the third pier (P3) that was part of an eight-span continuous structure, as shown in Fig. 2.2 (a). Details of the shape of the box girder and the failure location are presented in Fig. 2.2 (b) and (c). Four internal tendons and six external tendons were installed on either side of the box girder. The external and internal tendons had 15 and 19 seven-wire steel strands, respectively. The tendons were filled with cement grout. The strands consisted of one center wire with a radius of 2.6 mm and six outer wires with a radius of 2.5 mm, as shown in Fig. 2.2 (d) and (e).

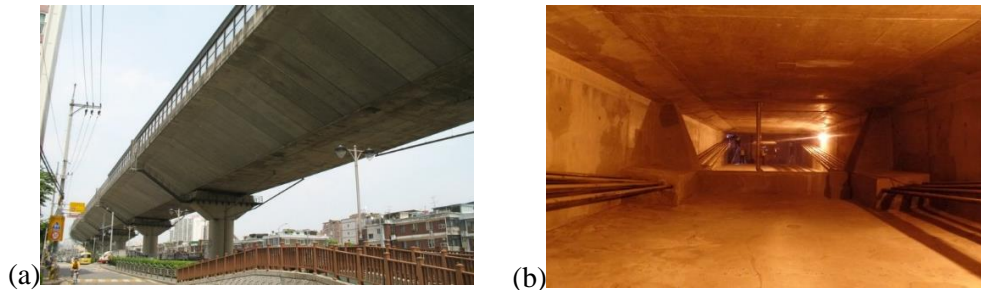


Fig. 2.1 The post-tensioned segmental concrete box-girder bridge (SMFMC 2017):
(a) typical view of outside box-girder ; and (b) typical view of inside box-girder

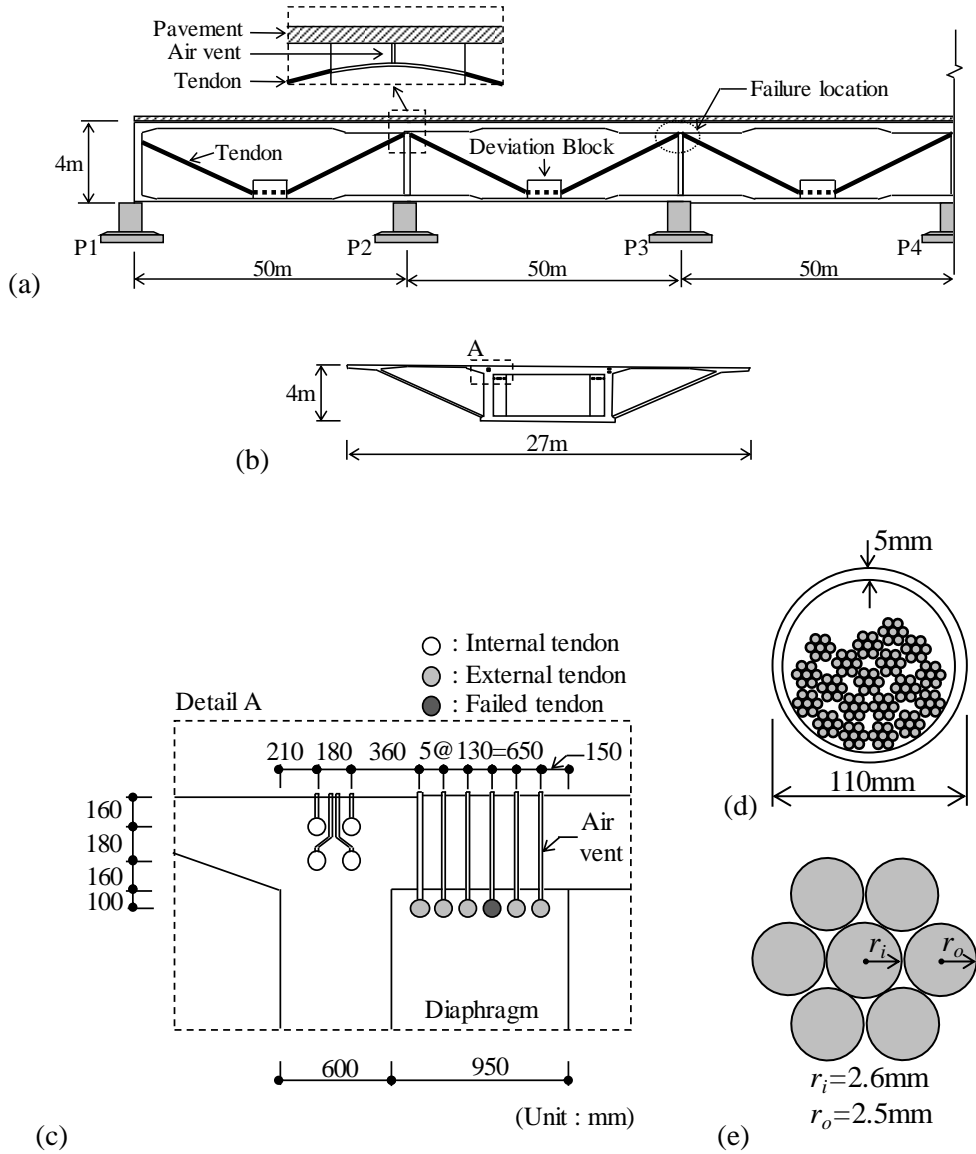


Fig. 2.2 Overview of the bridge: (a) side view; (b) section view; (c) close-up view of box A in (b); (d) cross-section of external tendon; and (e) cross-section of 7-wire steel strand

After the failure of tendons was observed, in-depth investigation including sounding inspection, borescope inspection, opening duct inspection and grout testing were performed for revealing the reason of the corrosion. From the investigation, the trace of bleed water and the void which are the result of the segregation were found. Some of the grout in tendon was shown as soft, chalky and visibly porous with having light color. The reason of grout problem may be resulted from high water-cement ratio revealed as 0.45 to 0.70 from grout testing. Also, the closer to air vent, the more chloride content was detected. At last, it was checked that the air vent penetrated.

By integrating the investigation results, corrosion in the strands occurred when chloride and water infiltrated the external tendon via air vents. As Fig. 2.2 (c) shows, the air vents were located above the saddle of the tendons towards the upper surface of the deck. Due to insufficient filling of grout at the saddle and air vents, large voids had formed in the tendons. When the pavement was replaced, a waterproofing layer was damaged, which resulting in the infiltration of chloride and water into the tendons through the air vents. After inspecting all the external tendons in the bridge, corrosion was detected in the strands of four out of six tendons in the section where the tendon failure had occurred. All the corroded tendons were replaced.

Samples of the corroded strands were gathered from the demolished tendons. The strands in the tendons were visually inspected and 21 pieces of corroded strands were collected. Each of the specimens were about 1.0 m in length.

2.2 Characteristics of Corroded Wires

Corrosion in metallic materials is generally examined by measuring the changes in weight (ASTM. 1999) or by measuring the corrosion depth using either a micrometer or a pit depth gauge (ASTM. 2005; Gonzalez et al. 1995). Decreases in the tensile strength of strands, however, cannot be examined by measuring weight changes or corrosion depth, because the strength is determined by the modulus of elasticity and the cross-section area. Therefore, alternative methods are needed to measure the section loss in corroded wires. Kashani et al. (2013) measured the cross-sections of corroded rebar using a 3-dimensional scanning optical measurement technique. The resolution of the scanner was 5 mega-pixels and the accuracy of the measurement was 20 μm , which was the highest resolution possible for the instrument. This method seemed to be a feasible solution for detecting the details of the shape of the cross-section of a corroded wire. However, it was not adopted because the scanner could capture only the partial surface of the outer wires.

2.2.1 Measurement of cross sections in corroded wires

The inner wire of strands was not visible, because it was surrounded by the outer wires. To measure the cross-sections of both inner and outer wires, specimens were cut, which exposed the corroded cross-sections. The cut section could then be accurately measured via photography. The collected strands were cut into 120 mm lengths whereas the completely unwound part of strand was not cut as shown in Fig. 2.3. The specimens were partially corroded along their length so that the corrosion was not apparent in all sections. There were 47 and 53 corroded and non-corroded

strand cross-sections, respectively.

All sections were photographed using a macro lens and a cell phone camera, as shown in Fig. 2.4. A 9× macro lens was clamped to the front of the cell phone camera to photograph sections of each wire and strand. Then, the section photos were imported to AutoCAD to gauge the section loss due to corrosion by measuring the corroded area. As shown in Fig. 2.5, the cross-section of an original wire was identified from three points in the boundary of the remaining section. The corroded surface was then drawn using a polyline. Finally, the hatched area in the figure was identified as the corroded area. This process was repeated for all the wires, and a corroded area of each wire was collected. Each wire was then catalogued according to the ratio of the corroded area and the area of the original section. This ratio will hereafter be referred to as the section loss.

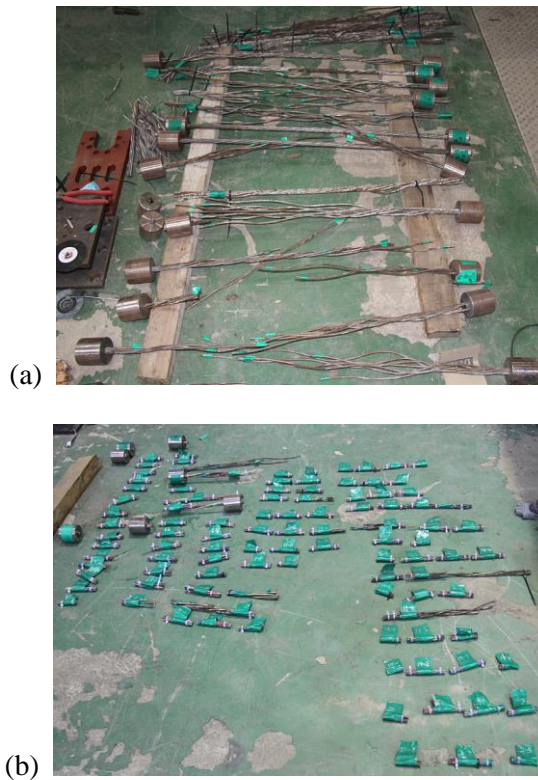
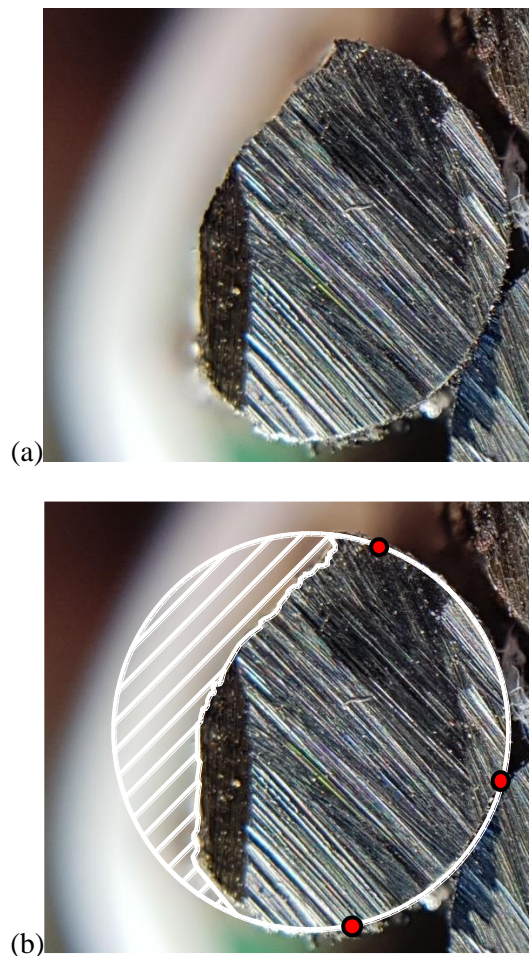
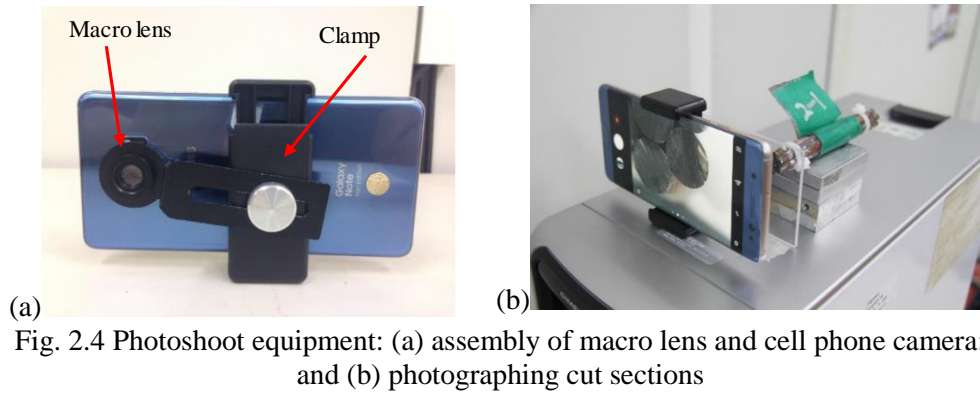


Fig. 2.3 Collected strands: (a) before cutting, (b) after cutting



2.2.2 Results of measurement

Fig. 2.6 shows the cross-sections of the corroded wires in states of minor to severe corrosion. The hatched areas represent corrosion. Once corrosion is initiated on a wire, it rapidly progresses in a circumferential direction rather than in a depth direction. This phenomenon probably happens because the chloride and the moisture simultaneously contact the outer surface of a wire when corrosion is initiated. In Fig. 2.2 (e), 2/3 of the surface of the outer wire is exposed and the remainder of the surface is hidden inside the strand. These corroded sections show that more than half of the surface was corroded with a section loss of about 20%, while the corrosion depth remained relatively shallow. As shown, the section loss was increased by continuous corrosion propagation along the surface. Simultaneously, corrosion gradually progressed in the depth direction of the wire. Based on this observation, the progress of corrosion in wires was identified and measured in two directions: circumferential and radial.

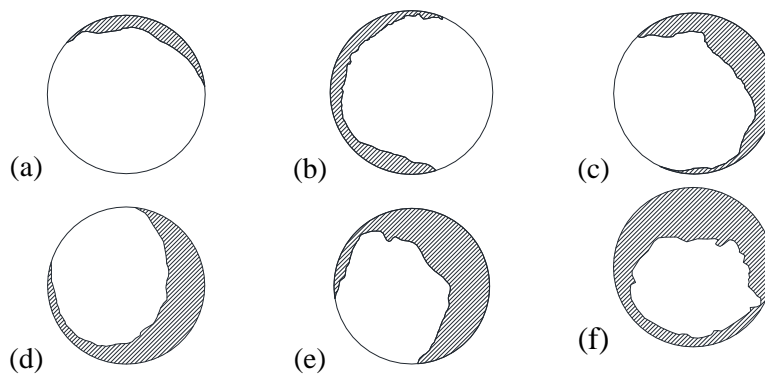


Fig. 2.6 Typical cross-sections of corroded wires: (a) section loss of 0% ~ 10%; (b) section loss of 10% ~ 20%; (c) section loss of 20% ~ 30%; (d) section loss of 30% ~ 40%; (e) section loss of 40% ~ 50%; and (f) section loss of 53%

The corrosion perimeters and depths of each of the wires were measured, as shown in Fig. 2.7. The corrosion perimeters were identified as L . If the corroded area was separated into two parts, each of the corrosion perimeters was measured. Corrosion depth was determined by the radial distance from the corroded surface to the original surface of the wire. Unlike the corrosion perimeter, corrosion depth varied along the corrosion surface. Thus, corrosion depth was measured by dividing the circumference of the original wire into 10,000 pieces, and then the maximum value among 10,000 corrosion depths was identified as p and defined as corrosion depth of wire.

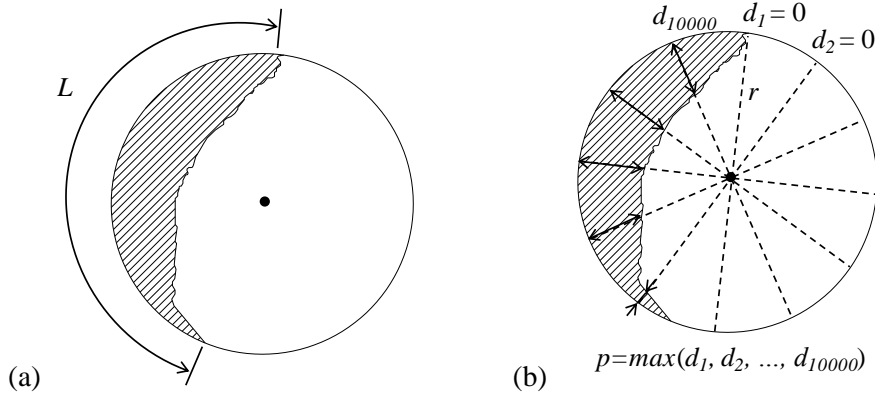


Fig. 2.7 Measuring corrosion properties: (a) corrosion perimeter; and (b) corrosion depth

Before analyzing the data for corrosion depths and perimeters, data from severely corroded strands were excluded. This was because the goal of this study was to evaluate the condition of the corroded tendons, and most of the inspected tendons showed only minor corrosion. Therefore, the inclusion of severely corroded strands could significantly skew the results.

When the tendon suffers corrosion, the actual stress of strand goes larger as the cross section of strand goes smaller. At last, the strand will fail when the actual stress exceeds the ultimate strength of strand as follows:

$$F = (1 - 0.01\eta_s) F_0 \leq f_{pe} A_0 \quad (2.1)$$

where η_s is the section loss in strand (%), F and F_0 are ultimate strength of corroded and original strand (N), respectively, f_{pe} is effective prestressing force of tendon (MPa), A_0 is the original cross sectional area of strand (mm²). The strand adopted in investigated bridge has 1,600 MPa of yield strength and 1,900 MPa of ultimate strength. Effective prestressing force of tendon is undefinable, but 80 and 85% of yield strength are used as the stress limit in AASHTO (2014) and KRTA (2016), respectively. As a result, the critical section loss of strand, $\eta_{s,c}$, which is the threshold of failure can be calculated as 28 and 33% for 80 and 85% of yield strength. In this regard, the upper limits for the section loss in strands was set at 25%. In addition, the tensile strength and elongation of the corroded strands was reduced significantly when the section loss was greater than 10% to 20% (SMFMC 2017). Therefore, the cross-sections of 137 corroded wires in 40 strands were investigated.

Variations in the corrosion depth and corrosion perimeter with respect to the section losses in wires are plotted in Fig. 2.8. For every section loss interval of 5%, the average and standard deviation of the corrosion depth and the corrosion perimeter were plotted. The corrosion depths and the corrosion perimeters were normal-

ized with respect to the radii and perimeters of non-corroded wires, respectively, because the radius of the inner wire was 0.1 mm larger than that of the outer wire. Although a larger scatter appeared for larger section losses, variations in both parameters with respect to the section loss were clear. Corrosion depth increased in an almost linear fashion as the section loss became larger, whereas the corrosion perimeter increased faster until the section loss reached approximately 10%. At a section loss of 10%, the corrosion perimeter reached approximately 50% of the wire's perimeter, as shown in Fig. 2.6.

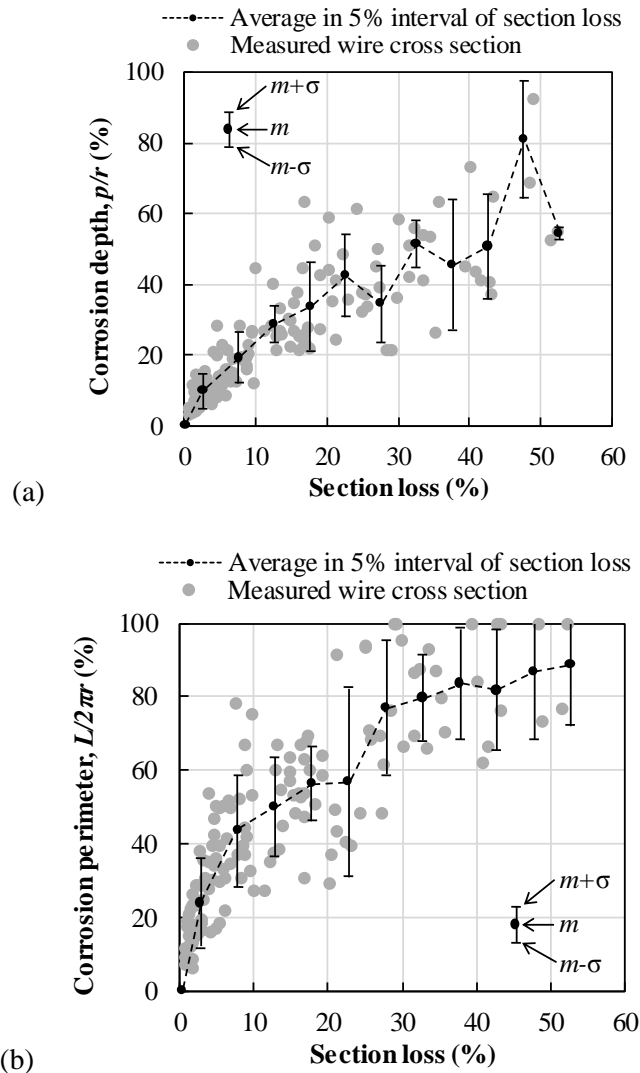


Fig. 2.8 Variations in corrosion shape with respect to section loss:
(a) corrosion depth; and (b) corrosion perimeter

2.3 Characteristics of Corroded Strands

2.3.1 Measurement of cross sections in corroded strands

Cross sections of strands were photographed with same procedure as in photographing wire. However, when the photograph of the whole section was taken, part of strand was distorted or out-focused in image, as shown in upper right of Fig. 2.9 (a), as the distance from the focus of camera increases. That is, it was challenging to identify the corroded area by only the photographs of strand. For a detailed analysis, photographs of each wire were taken first and assembled based on the photographs of strand by importing those into AutoCAD. Therefore, photographs of each wire taken in previous chapter were assembled based on the photograph of strand. Eventually, corroded area in a strand section was identified as a hatched region in Fig. 2.9 (b). This process was repeated for all the strand cross sections. Owing to the high forces stressed on tendon, twisting force was released and the locations of each wire were slightly rumped. Thus, positions of each wire were arranged to be a regular hexagon around the center wire. Total 26 corroded strand cross sections were obtained including 85 corroded wire cross-sections. The number of investigated strand cross sections is smaller than that of investigated strand cross sections in photograph of wire because there are completely rumped strand cross sections during cutting the strand.

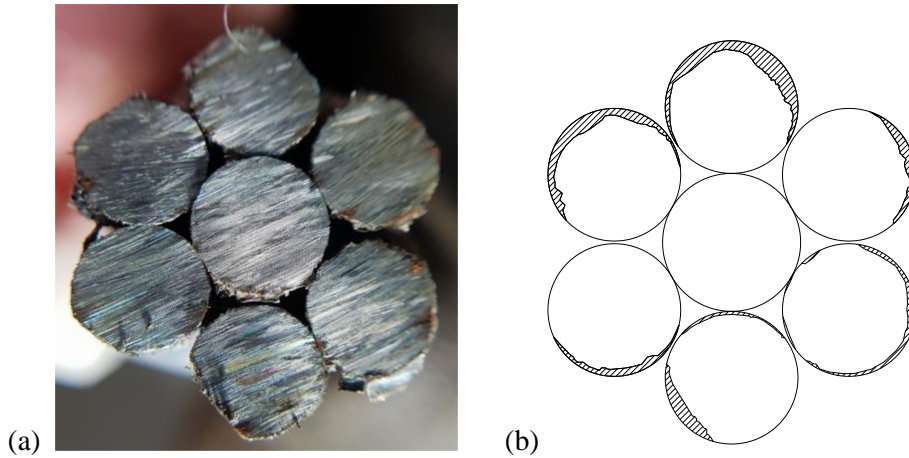


Fig. 2.9 Cross-section of a corroded strand: (a) photograph of a corroded strand section; and (b) identified cross-section.

2.3.2 Visible and invisible region

It is not feasible to visually inspect the inside of a strand because the center wire is completely surrounded by six outer wires. This invisible region can be defined by a hexagon, which is formed by connecting the centers of the outer wires, as shown in Fig. 2.10. Evaluating section loss in corroded strand can only be performed based on the information obtained from the visible region.

Of the 26 cross-sections examined, corrosion in wires that was completely hidden in the invisible region was found in five of the cross-sections, as shown in Fig. 2.11. It should be noted that cases were not counted if the section loss in the invisible region originated from the visible region, because the section loss of those cases can be visualized. The section losses in each wire for these strands are tabulated in Table 2.1. Wire 1 in outer wire is the most severe corroded wire among outer wires and assigned in top of the strand. The section losses listed in the table were measured according to the corroded area with respect to the nominal cross-sectional area of a strand. With the exception of the strands shown in Fig. 2.11 (a),

all the center wires showed corrosion. It is interesting that the corroded areas occurred in invisible regions located adjacent to each other. That result indicates that stagnating corrosion inducers inside the strands simultaneously initiated corrosion. The amount of section loss in the invisible regions ranged from 0.1 to 2.5%, and this amount increased as total section loss increased.

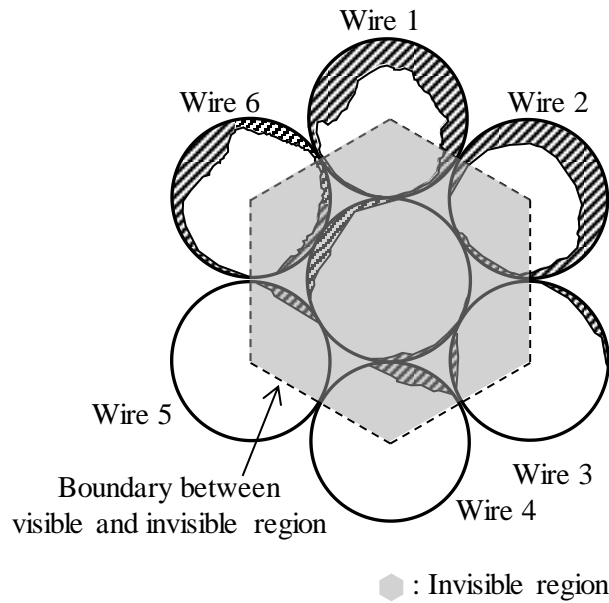


Fig. 2.10 Identifying visible and invisible regions in the cross-section of a corroded strand

Table 2.1 Section Losses in Each of the Wires Presented in Fig. 2.10

Fig. 2.11	Section loss of wires (Section loss ratio versus strand, %)							
	Center wire	Outer wire						Total
		1	2	3	4	5	6	
(a)	-	0.7%	0.2%	-	-	0.1%	0.1%	1.1%
(b)	0.1%	0.9%	0.2%	-	-	-	-	1.3%
(c)	0.8%	0.2%	-	0.7%		0.3%	-	2.0%
(d)	1.3%	3.7%	0.5%	0.6%	1.1%	0.6%	-	7.7%
(e)	1.4%	5.5%	4.7%	0.7%	0.7%	0.4%	3.5%	16.8%

* Bolded section loss of wire means corrosion of invisible region.

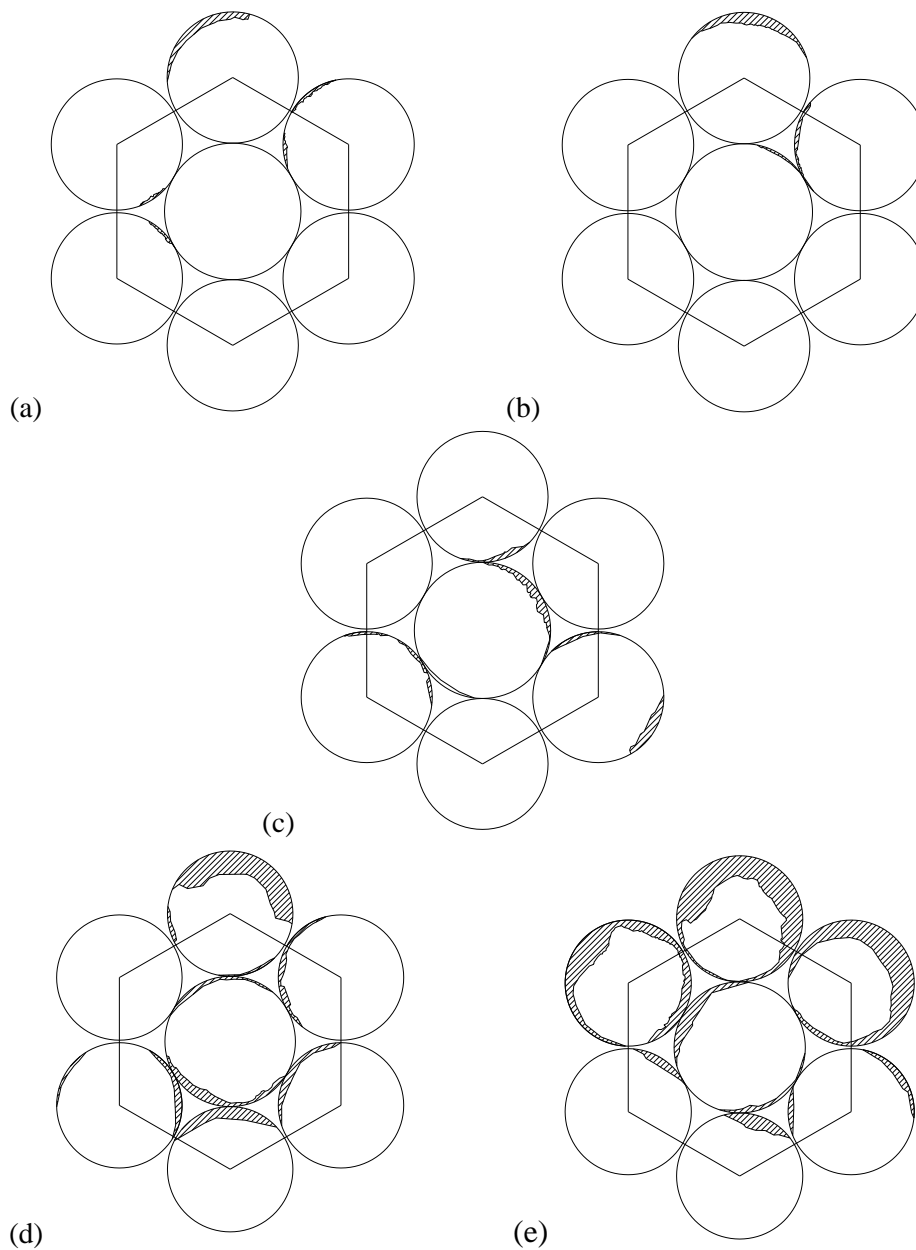


Fig. 2.11 Cross-sections of strands corroded in the invisible region: (a) section loss of 1.1%; (b) section loss of 1.3%; (c) section loss of 2.0%; (d) section loss of 7.7%; and, (e) section loss of 16.8%

2.3.3 Corrosion depth and perimeter in strand

In the analysis of corroded wires, section loss in a corroded wire could be estimated via the Proposed models I and II by establishing the corrosion depth and perimeter. The feasibility of applying these models for estimating section loss in corroded strands was reviewed. Actual section loss in a strand was plotted for the mean corrosion depths and mean corrosion perimeters, as shown in Fig. 2.12. The mean corrosion depths and perimeters were determined by averaging the measurements in each wire obtained from the visible region. Correlations were drawn between the actual section loss in corroded strands and the mean of the measurements. Therefore, section loss in corroded strands could be determined from the corrosion depth and perimeter, although corrosion in the invisible region would not be inspected.

Dispersion in section loss per corrosion perimeter was greater than that per corrosion depth. That result could be explained by observation of the corroded wires. Yoo et al. (2018) found that the corrosion in a wire progresses along the perimeter direction of a wire faster than its depth direction when corrosion is initiated. Therefore, corrosion in a wire can easily progress to the invisible region, which would limit the measurement of corrosion on the perimeter. On the other hand, corrosion depth generally measured near the center of a corroded area begins in the visible region, because the wire surface in the visible region is likely to be more exposed to corrosion inducers such as moisture and chloride ions.

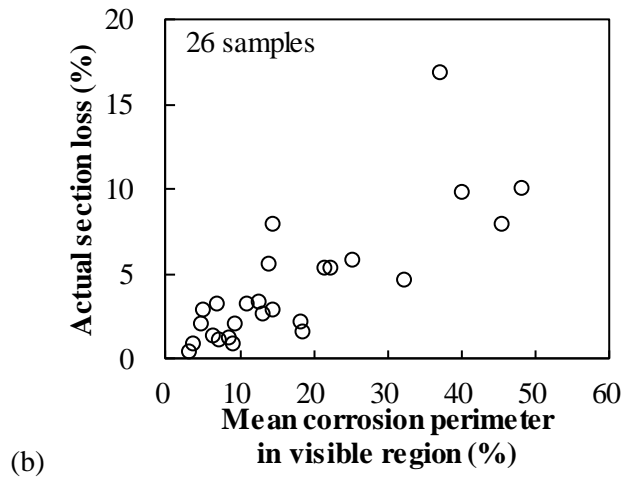
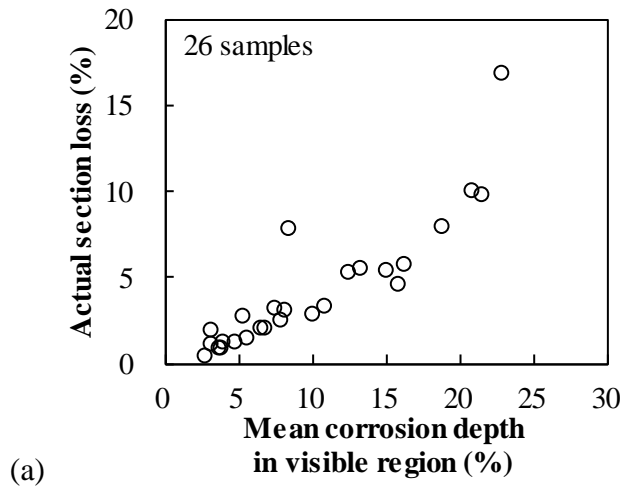


Fig. 2.12 Section losses of corroded strands with respect to the following: (a) mean corrosion depth in the visible region; and (b) mean corrosion perimeter in the visible region

2.3.4 Number of corroded outer wires

Counting the number of corroded wires is a convenient way to evaluate the significance of corrosion in strands as a preliminary inspection. Section losses of strands with respect to the number of corroded wires were identified from the visible region and are plotted in Fig. 2.13. Since the center wire is invisible, only the outer wires could be counted. The results show that section loss in corroded strands definitely increases as the number of corroded wires increases. All corroded strands in the visible region could be identified, and none of the cross-sections were corroded only in the invisible region. That result shows that section loss was less than 5% when fewer than three corroded wires were identified in the visible region.

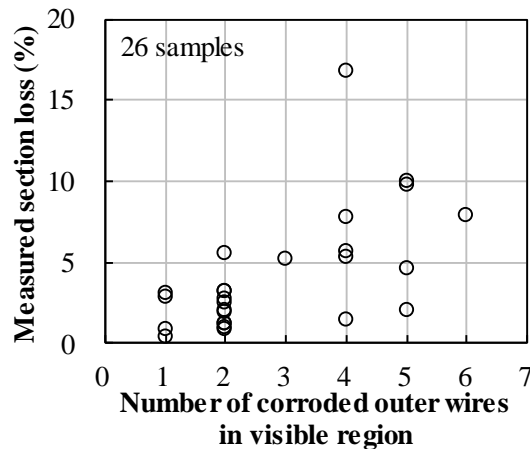


Fig. 2.13 Section losses of corroded strands with respect to the number of corroded outer wires identified in the visible region

CHAPTER 3

Modeling Corrosion Progress of Steel Wires in External Tendon

When prestressing tendons are corroded, a bridge owner must decide whether to replace or repair them. If this decision must be based on a destructive inspection method, section losses in the steel strands must be estimated either by measuring the corrosion depth or by measuring the perimeter of the corrosion area. For this study, models for the determination of corrosion progress in corroded wires were investigated in a preliminary study of evaluating section losses in strands.

Analysis showed that using models of existing corrosion progress routinely underestimated the section losses for corrosion depth. Actual measurements showed that corrosion rapidly progressed along the perimeter in the earlier stages, and the result was a corroded surface with a convex shape. Herein, new corrosion models that more accurately reflect the actual corroded sections of wires are proposed. Although the measurements showed a large degree of dispersion, the proposed models were verified as more effective in estimating section losses.

3.1 Corrosion Model of Wires using Corrosion Depth

3.1.1 Existing corrosion models

Although the remaining area of a corroded section is of interest, cutting wires is impossible while a bridge is in service. Therefore, section loss in wires must be estimated via measurement of either the corrosion depth or the corrosion perimeter on the surface of wires. The correlations could be numerically established by conducting regression analysis using measurements. As in the present study, however, it is questionable whether only 137 measurements with a large scatter could confirm the validity of this type of regression analysis. As an alternative, the adoption of a corrosion model was attempted to idealize the progression of corrosion in a wire to offer a better choice for estimating section loss via measurements.

Val and Melchers (1997) first introduced a corrosion model for rebar. Due to similarities in the shape of rebar and wires, this model has been adopted to simulate pitting corrosion in wires (Darmawan and Stewart 2007; Guo et al. 2010). As shown in Fig. 3.1 (a), this model assumes that corrosion pits take a hemispherical form. The center of the hemisphere is always fixed at the top, and corrosion progresses radially. Thus, the corrosion depth is the same as the radius of the corrosion pit. According to this model, the corroded area, $A_{SL,1}$, can be calculated by using the corrosion depth, p , as follows.

$$A_{SL,1} = r^2 (\theta_1 - \sin \theta_1 \cos \theta_1) + p^2 (\theta_2 - \sin \theta_2 \cos \theta_2) \quad \text{for } 0 \leq \theta_1 \leq \pi \quad (3.1)$$

In that equation, r is the radius of a wire and θ_1 and θ_2 are functions of p , as defined below.

$$\theta_1 = \arccos \left(1 - \frac{p^2}{2r^2} \right) \quad (3.2)$$

$$\theta_2 = \arccos\left(\frac{p}{2r}\right) \quad (3.3)$$

The range of p is from zero to $2r$ and the corresponding θ_1 ranges from 0° to 180° .

The entire area of the wire is defined as corroded when p reaches $2r$ and θ_1 is 180° .

Another corrosion model recently proposed by Hartt and Lee (2016) assumed that corrosion progresses in a planar shape, as shown in Fig. 3.2 (b). As per the observations presented in a previous chapter and in Fig. 2.6, this model seems more realistic because the shape of the corroded area was spread over the entire surface of the wire. The corroded area, $A_{SL,2}$, can be defined in terms of p as follows.

$$A_{SL,2} = r^2 (\theta_1 - \sin \theta_1 \cos \theta_1) \text{ for } 0 \leq \theta_1 \leq \pi \quad (3.4)$$

θ_1 is defined below.

$$\theta_1 = \arccos\left(1 - \frac{p}{r}\right) \quad (3.5)$$

The range of p is from zero to $2r$, and the corresponding range of θ_1 is from 0° to 180° . When corrosion depth, p , reaches $2r$, θ_1 becomes 180° , which represents a completely corroded wire.

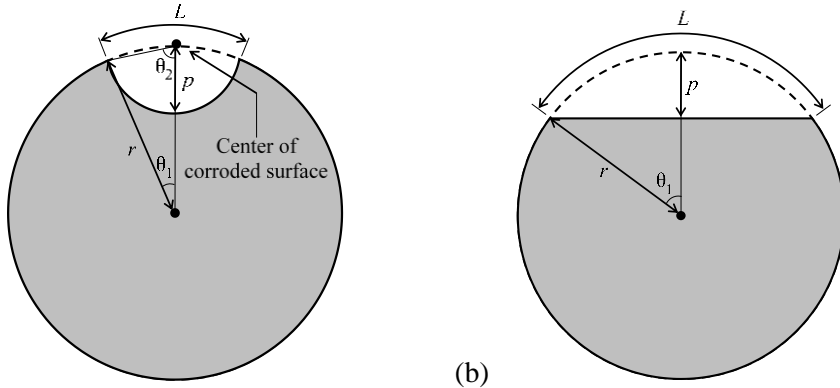


Fig. 3.1 Configuration of idealized corrosion: (a) Val and Melchers' model (1999); and (b) Hartt and Lee's Model (2016)

Comparison of the measured and estimated section losses was used to validate the models. Section losses were plotted with respect to the corrosion depth, as shown in Fig. 3.2. Comparing the estimates with the measured data shows that both models consistently underestimated the section loss for corrosion depth. In particular, with one exception, all measured section losses were greater than Val and Melchers' model. This was because the corrosion areas were not in the shape of pitting corrosion but appeared more as general corrosion. As a result, the section loss corresponding to corrosion depth was underestimated. On the other hand, Hartt and Lee's model also underestimated the section losses, but their model provided a better correlation with the measured data. As shown in Fig. 2.6, corrosion simultaneously progressed along the circumferential and radial directions of the wires. This observation indicates that the shape of the remaining surface will be convex rather than either concave or planar.

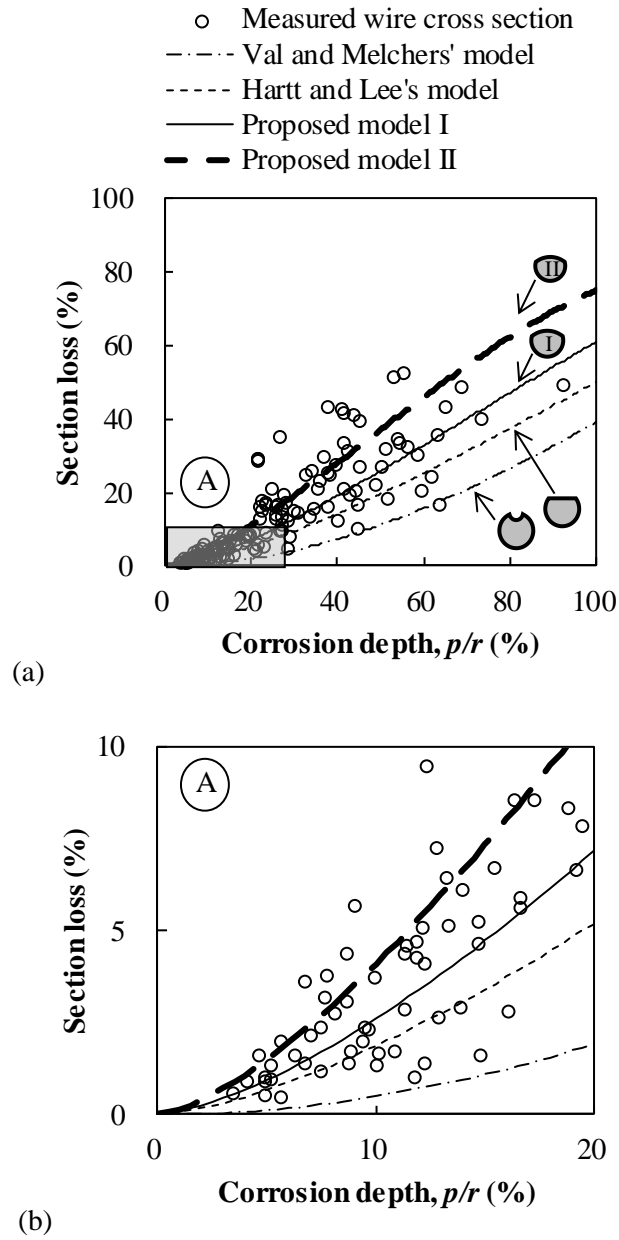


Fig. 3.2 Comparison between measured corroded wire sections and corrosion models: (a) section loss versus corrosion depth; and (b) zoom in of box A

3.1.2 Proposed corrosion model I

These observations led to the development of a new corrosion model that would simulate the actual shape of corroded wire sections. The new corrosion model shown in Fig. 3.3 was proposed to provide a better estimate of section loss with respect to the corrosion depth. The proposed model assumes the corrosion surface is rounded with the center fixed at the perimeter of the wire, which results in a convex shape for the corroded surface. These assumptions assume a corrosion perimeter, L , that is greater than that of the existing models, which allows a more accurate estimation of corrosion depth. The advantage of this model is that the shape of the remaining section approximates the actual cross-section of a wire, which provides the corrosion depth for a larger section loss and should provide a better correlation of the measurements. Estimates for corroded areas, $A_{SL,3}$, for corrosion depth, p , can be obtained using the equations shown below.

$$A_{SL,3} = r^2 (\theta_1 - \sin \theta_1 \cos \theta_1) - s^2 (\theta_2 - \sin \theta_2 \cos \theta_2) \text{ for } 0 \leq \theta_1 \leq \pi \quad (3.6)$$

where, s , θ_1 and θ_2 can be calculated as follows.

$$s = 2r - p \quad (3.7)$$

$$\theta_1 = 2\theta_2 \quad (3.8)$$

$$\theta_2 = \arccos\left(\frac{s}{2r}\right) \quad (3.9)$$

Similar to the existing models, the corrosion depth, p , ranges from zero to $2r$ and the corresponding θ_1 ranges from 0° to 180° . When the corrosion depth, p , reaches $2r$, θ_1 becomes 180° , which means the entire area of the wire is corroded.

The proposed corrosion model appears in Fig. 3.2 labeled as ‘Proposed model I’. This model provided a better estimate for the section loss with respect to the

corrosion depth. Estimates for the residuals of the section loss were based on both the existing and proposed models and are plotted in Fig. 3.4. Residuals are calculated by subtracting the measured section loss from the estimated section loss corresponding to the corrosion depth. The results show that the Val and Melchers' and Hartt and Lee's models gave mean values for the residuals of about 9.8% and 5.6%, respectively. The residuals from the Proposed model I were evenly distributed from zero with a mean of about 2.7% and a standard deviation of 7.3%, which were the least of the average and standard deviation values.

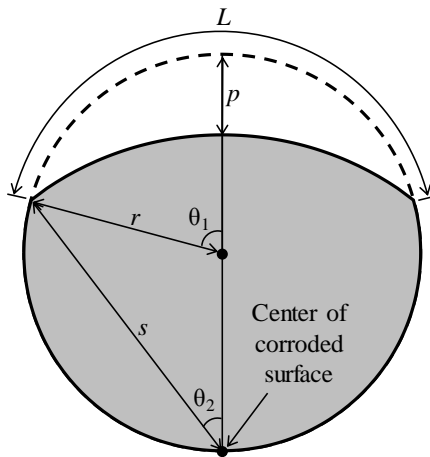
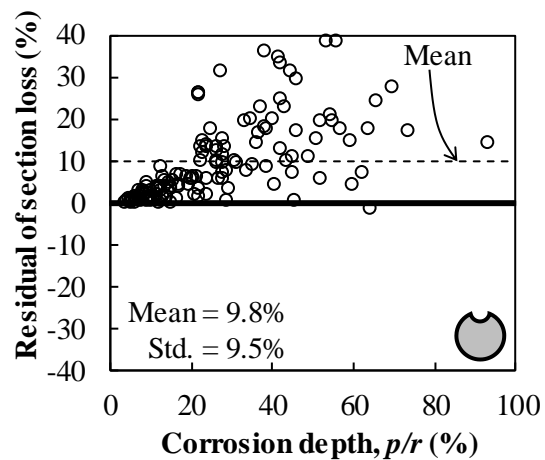
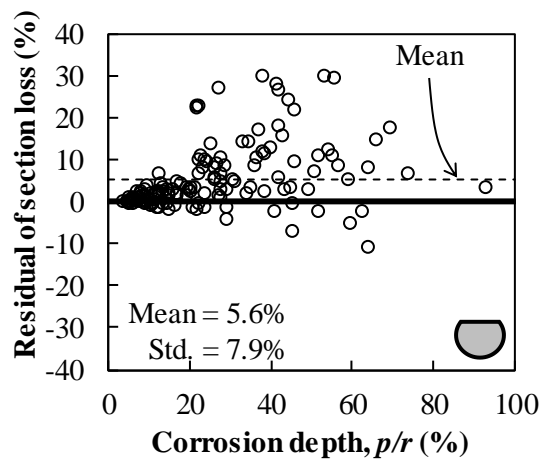


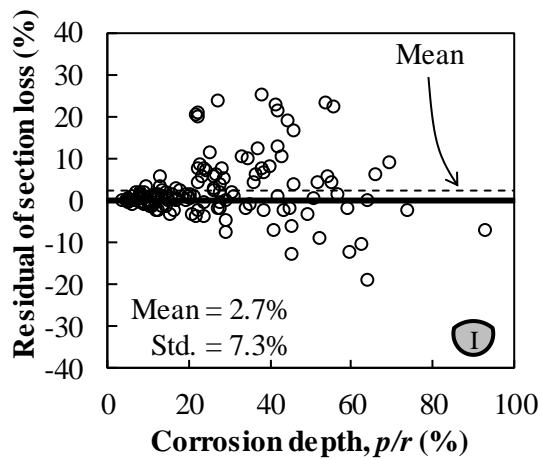
Fig. 3.3 Configuration of Proposed corrosion model I



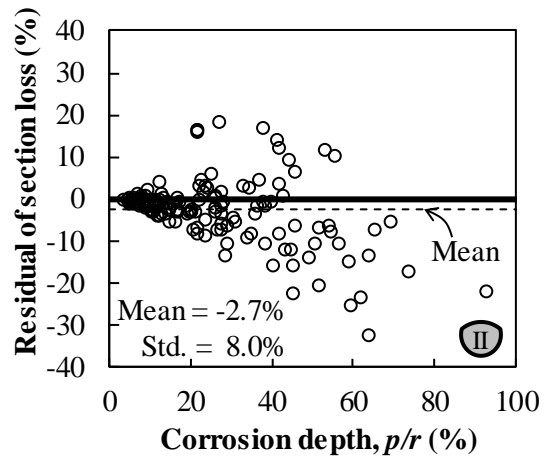
(a)



(b)



(c)



(d)

Fig. 3.4 Comparing residuals of section loss for each model: (a) Val and Melchers' model; (b) Hartt and Lee's model; (c) Proposed model I; and (d) Proposed model II

3.2 Corrosion Model of Wires using the Corrosion Perimeter

Conventionally, the severity of corrosion damage in a wire is measured according to the corrosion depth (Faroz et al. 2016; Li et al. 2014; Shibata 1991; Torres-Acosta and Martinez-Madrid 2003; Tuutti 1982), particularly the depth of the maximum corrosion. To measure the correct corrosion depth while a bridge is in service, the corrosion products and the cement grout should be completely removed after opening the duct. The corrosion depth can then be measured using pit gauges. To obtain corrosion depth, as many measurements as possible should be performed for finding the maximum value. If the strand is corroded across a larger area, finding the maximum value of corrosion depth may not be effective, and measuring the corrosion perimeter could be an alternative that would be easier to visually identify. The corrosion perimeter can be measured by inserting an endoscope or a borescope into the tendon. Only a small hole is needed to insert these devices, and the corrosion perimeter could be measured visually without either the use of additional devices or the need to remove the corrosion products. The applicability of using the corrosion perimeter to estimate section loss in a wire was verified using both the existing and the proposed corrosion models.

3.2.1 Corrosion models with corrosion perimeter

Measures of the corrosion perimeter and the corresponding section loss are plotted with the estimates of section loss for three corrosion models in Fig. 3.5. This figure demonstrates how all corrosion models significantly overestimate the corrosion perimeter. The overestimation was less for Proposed model I compared with the other models, but even this model gave a significant residual as the corrosion perimeter became larger. All models estimate a complete section loss when the corrosion perimeter reaches 100%. However, as Fig. 4 shows, a section could remain even when the entire wire surface is corroded. Therefore, both the existing models and Proposed model I are not applicable for estimating section loss using the corrosion perimeter.

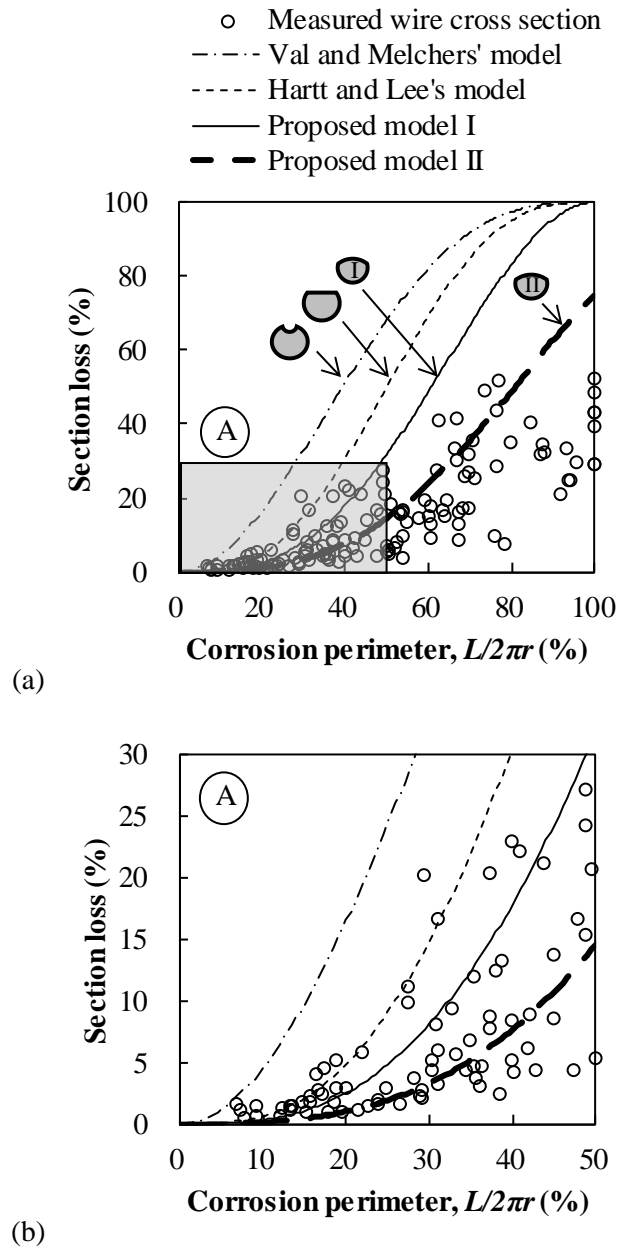


Fig. 3.5 Comparison between measured corroded wire sections and corrosion models: (a) section loss versus corrosion perimeter; and (b) enlargement of box A

3.2.2 Proposed corrosion model II

The reason of the overestimation at the aforementioned models is the assumption adopted in those models. Both the existing models and the Proposed model I commonly adopts the assumption that corrosion propagates from a fixed point. This fixed point is identified in Fig. 3.1 and Fig. 3.3 as the center of the corroded surface. Since this point is fixed on the surface of a wire, 100% of the corrosion perimeter must correspond to a complete section loss, although the section loss for 100% of the corrosion perimeter in the measured data was about 30% to 50%. If this constraint is released, a better estimate could be expected.

The assumption related with the fixed center makes existing the only one corroded surface to the one corrosion depth. In other words, the assumption maintains the one-to-one correspondence between corrosion depth and perimeter. For releasing this constraint, the alternative for defining this relationship is required.

Releasing the constraint could be achieved by adopting the assumption that the corrosion propagates from a floating point. The role of this point is also the center of the corroded surface. Floating position of the corroded surface center could be achieved by establishing a relationship between the corrosion depth and the corrosion perimeter based on measured data. In Fig. 3.6, the corrosion perimeter is plotted with respect to the corrosion depth for all wires. Although the figure shows a large degree of variability, it shows how a larger corrosion depth corresponds to a larger corrosion perimeter. Due to a large degree of variability in the data, the relationship between two parameters was established by averaging the corrosion perimeters in 10% intervals of the corrosion depth. Regression analysis was then performed for the averaged corrosion perimeters and the corrosion depth. Performing regression analysis on the raw data would lend weight to results by virtue of a

greater number of data points. Thus, averaging for 10% intervals of the corrosion depth was conducted to avoid the weighting issue. The relationship between the corrosion perimeter and the corrosion depth was determined as follows.

$$\frac{L}{2\pi r} = \left(\frac{p}{r}\right)^{0.49} \quad (3.9)$$

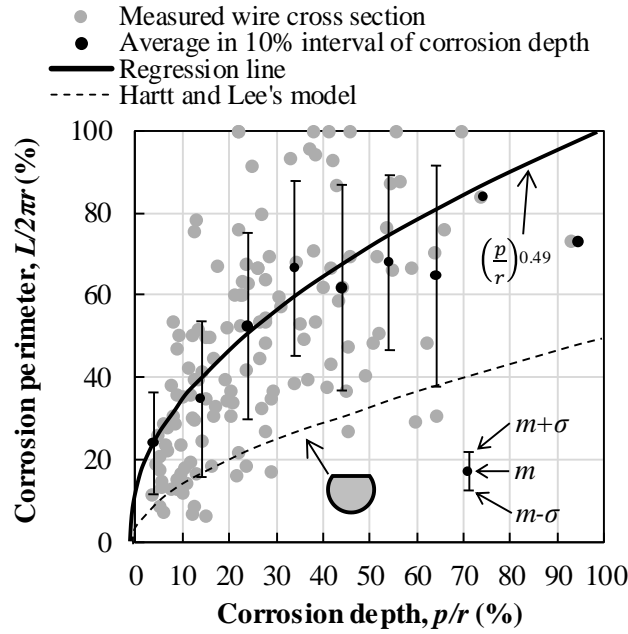


Fig. 3.6 Regression analysis results between averaged corrosion depth and corrosion perimeter

The definition for a corroded area in the modified model, which is hereafter referred to as Proposed model II, is almost identical to that for Proposed model I as shown below because both models assumes a convex shape for the corrosion surface.

$$\begin{cases} A_{SL,4} = 0 & \text{for } \theta_1 = 0 \\ A_{SL,4} = r^2 (\theta_1 - \sin \theta_1 \cos \theta_1) - s^2 (\theta_2 - \sin \theta_2 \cos \theta_2) & \text{for } 0 < \theta_1 \leq \pi \end{cases} \quad (3.10)$$

The difference between Eq. (3.6) and (3.9) is occurred from the floating position of corrosion surface center. When there is no corrosion, the center of corrosion surface can be everywhere which means indeterminate. The other factors in Eq. (3.10) such as θ_2 and s cannot be calculated because these factors are calculated based on the geometric shape of given corrosion surface center. Therefore, the calculation of zero section loss is separately defined in Eq. (3.10). The definitions of θ_1 , θ_2 and s were modified to reflect the relationships in Eq. (3.9), as shown below.

$$\theta_1 = \frac{L}{2r} = \pi \left(\frac{p}{r} \right)^{0.49} \quad (3.11)$$

$$\theta_2 = \arccos \left[1 + \frac{p^2 - 2rp}{2s[s - (r - p)]} \right] \quad (3.12)$$

$$s = r + \frac{p^2 + 2rp \cos \theta_1}{2r(1 + \cos \theta_1) - 2p} \quad (3.13)$$

A configuration of this model is presented in Fig. 3.7. The corroded area per this model can be determined if one of the corrosion depths, p , or the corrosion perimeter, L , is measured. If L is measured, p can then be determined by Eq. (3.9). Other variables can then be obtained from Eqs. (3.11), (3.12) and (13). In the early stages of corrosion, the center of the corroded surface is located near the perimeter

of the wire. As corrosion progresses, its center moves toward the center of the wire. When the entire surface of a wire is corroded, the center is at a quarter of the depth of the wire, and the section loss becomes 75%. It should be noted that the existing models, as well as Proposed model I, dictate that a wire would be considered completely corroded when the corrosion perimeter reaches 100%. As shown in Fig. 2.7 (f), this model simulates more realistic conditions for a corrosion perimeter of 100%.

Estimation results are presented in Fig. 3.2 and Fig. 3.5, and residual plots are shown in Fig. 3.4 and Fig. 3.8. The results show that releasing the center of the corroded surface was effective when the section loss was estimated based on the corrosion perimeters. Although regions with larger corrosion perimeters continue to produce larger errors in estimation, the proposed model II provided the best overall results with a mean residual section loss of only 5.2%, whereas the mean residuals of other models were greater than 20%. When the section loss was estimated from the corrosion depth using the Proposed model II, which is shown in Fig. 3.2 and Fig. 3.4 (d), the section loss was over-estimated. Thus, the Proposed model II is suitable for estimating section loss when the corrosion perimeter is used, whereas the Proposed model I provides a better estimation when using the maximum corrosion perimeter. Fig. 3.9 shows cross-sections of existing and proposed models and typical measured sections for the section losses of 10%, 30% and 50%. Comparing the loss in each of the cross-sections clearly validates the use of a convex shape for the modeling of a corroded surface.

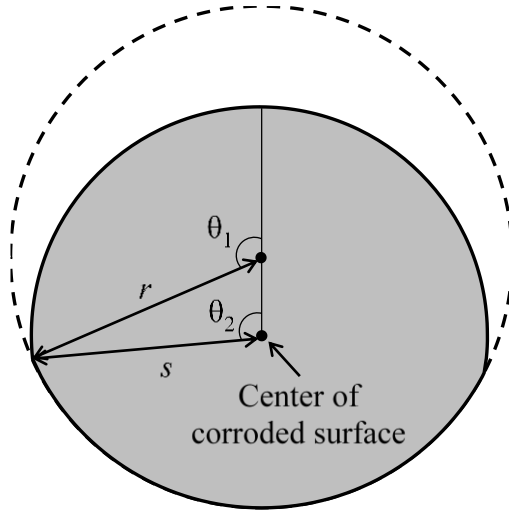
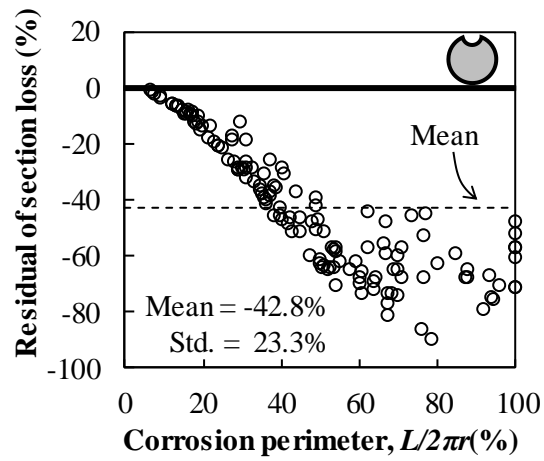
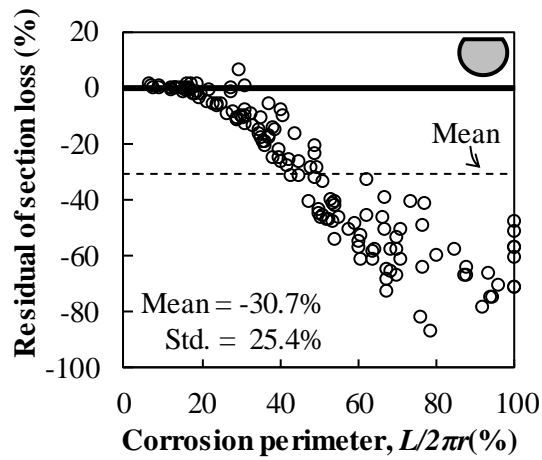


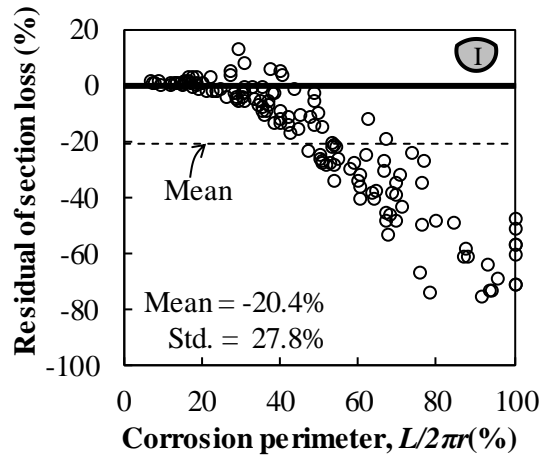
Fig. 3.7 Configuration of Proposed corrosion model II



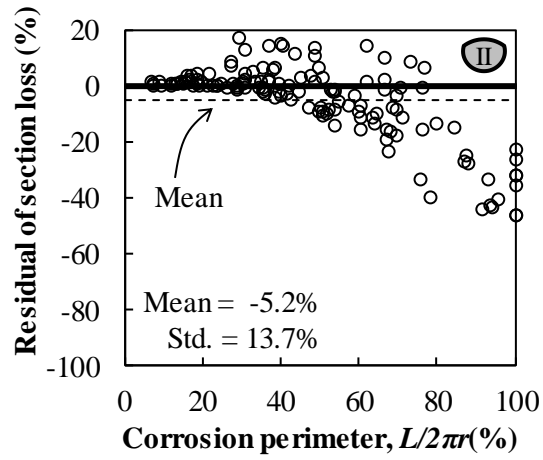
(a)



(b)



(c)



(d)

Fig. 3.8 Comparing residuals of section loss for each model: (a) Val and Melchers' model; (b) Hartt and Lee's model; (c) Proposed model I; and (d) Proposed model II

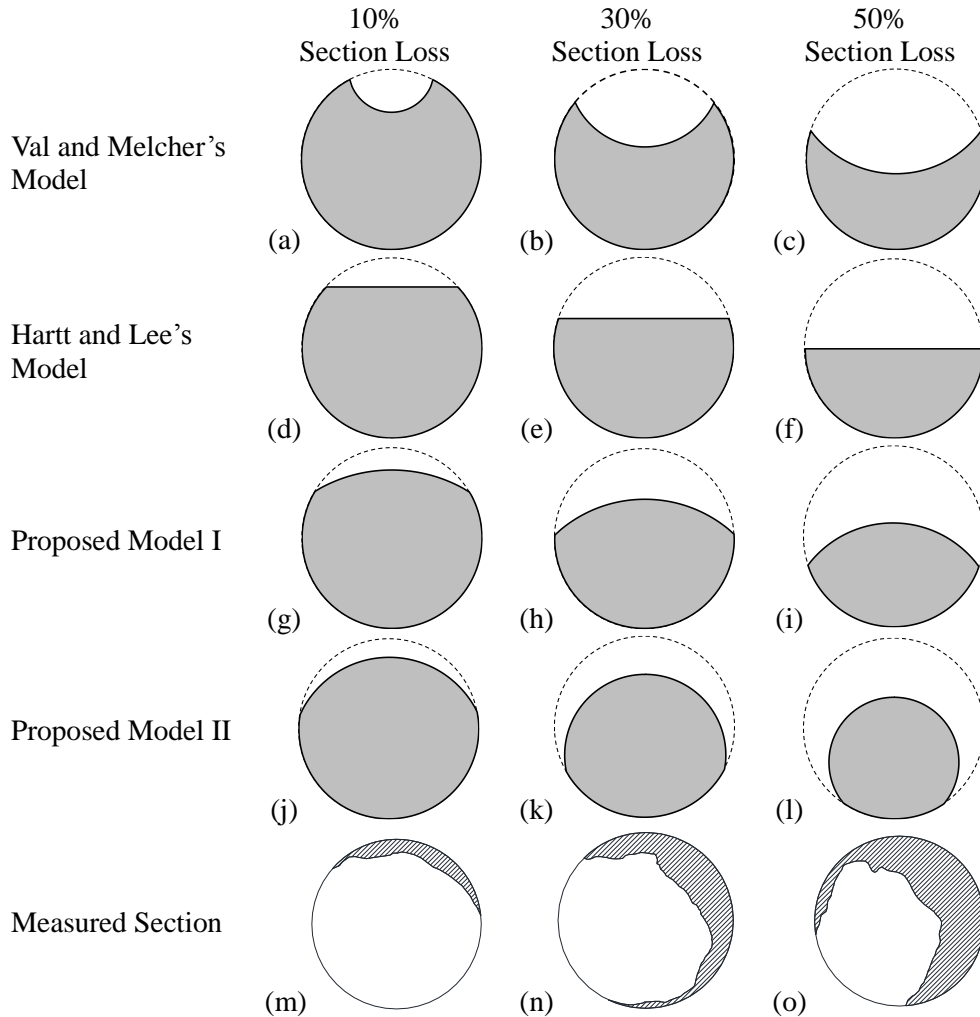


Fig. 3.9 Comparing cross-sections of each model and measured section for the section losses of 10%, 30% and 50%: (a) 10% section loss of Val and Melchers' model; (b) 30% section loss of Val and Melchers' model; (c) 50% section loss of Val and Melchers' model; (d) 10% section loss of Hartt and Lee's model; (e) 30% section loss of Hartt and Lee's model; (f) 50% section loss of Hartt and Lee's model; (g) 10% section loss of Proposed model I; (h) 30% section loss of Proposed model I; (i) 50% section loss of Proposed model I; (j) 10% section loss of Proposed model II; (k) 30% section loss of Proposed model II; (l) 50% section loss of Proposed model II; (m) 10% section loss of a typical measured section; (n) 30% section loss of a typical measured section; and (o) 50% section loss of a typical measured section

3.2.3 Limitation of Proposed model II

The estimated section loss in wire from Proposed model II shows a certain bias as the corrosion perimeter increases. The reason of this bias comes from the fitted relationship between the corrosion depth and the corrosion perimeter. This relationship is difficult to be defined as can be seen in Fig. 3.6. When the corrosion depth reaches 10%, the range of corrosion perimeter becomes 10% to 80%. Furthermore, there is a only limited number of samples which have a corrosion depth larger than 60%. These reasons hinder the fitness of proposed model II in terms of section loss in wire.

For solving these hindrances, the target range of fitting is changed to focus on narrow region. Moreover, the model used in regression analysis should contain larger degree of freedom than that of exponential function for increasing the fitness of regression model. In this respect, polynomial form of fitting function is adopted with modified target range for identifying the effect of regression model.

The target range of section loss in strand is determined in Eq. (2.1) by considering effective prestressing force. In this examination, one more factor is considered for narrowing the target range of section loss in strand. This factor is strength degradation effect by section loss in strand which will be fully explained in chapter 4 and means that the ultimate strength of corroded strand, F , decreases more than the section loss in strand. The equation with strength degradation effect obtained by Jeon et al. (2017) is derived as follows:

$$F = (1 - 0.01306\eta_s) F_0 \leq f_{pe} A_0 \quad (3.14)$$

The effective prestressing force is considered as 90% of yield strength for the conservative evaluation. The critical section loss of strand, $\eta_{s,c}$, is computed as 17.4%

which is more conservative range than previous range of 25%. As the target range is changed, the wire samples in the strand within the target range is also changed. As shown in Fig. 3.10, the most of wire samples sorted out by newly determined target range have a longer corrosion perimeter than 40%.

The regression analysis is performed on the new target range. The regression model is set as polynomial form. Because there is no corrosion depth and perimeter when there is no corrosion, the model should pass through origin. Also, the regression model should be monotone increasing. All of this constraint are expressed in formulation as Eqs. (3.15) ~ (3.17).

$$\text{Regression model : } y = b_0 + b_1x + \dots + b_nx^n \quad (3.15)$$

$$\text{Equality constraint : } b_0 = 0 \quad (3.16)$$

$$\text{Inequality constraint : } \frac{dy}{dx} = b_1 + 2b_2x + \dots + nb_nx^{n-1} \geq 0 \quad (3.17)$$

The degree of polynomial is determined by cross-validation (James et al. 2013) as shown in Fig. 3.11. Based on the value of cross-validation, the degree of polynomial is determined as third degree polynomials as written in Eq. (3.18) and drawn in Fig. 3.12.

$$y = 3.36x - 0.063x^2 + 0.00039x^3 \quad (3.18)$$

The section loss in wire can be estimated based on polynomial form of relationship between corrosion depth and perimeter. The procedure of calculating the section loss in wire is same with Proposed model II. The calculated section loss is presented in terms of corrosion depth and perimeter, respectively, in Fig. 3.13 (a) and (b). The results show that the section loss in wire estimated from the polynomial regression is worse than that from the exponential regression. That is, the estimated result is not improved by the regression line of polynomial form which

have more degree of freedom than exponential form. In other word, well-fitted line in corrosion depth and perimeter does not guarantee the better estimation result. In this regard, there is a limitation in the geometric model-based estimation.

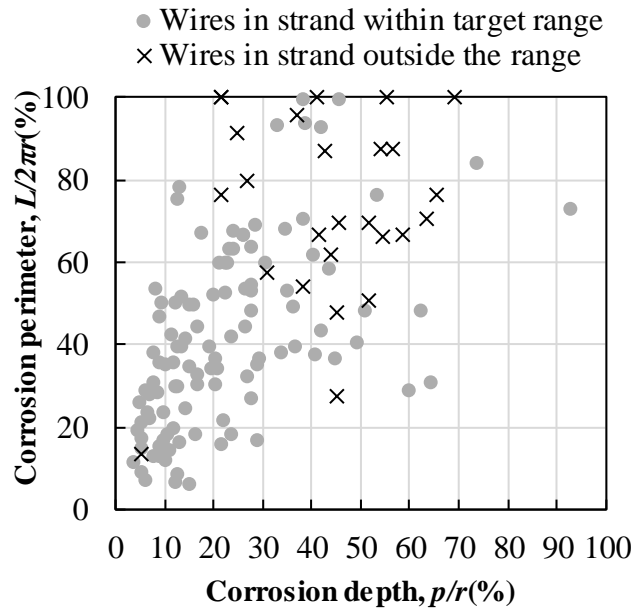


Fig. 3.10 Corrosion depth and perimeter of wires in strand by the target range

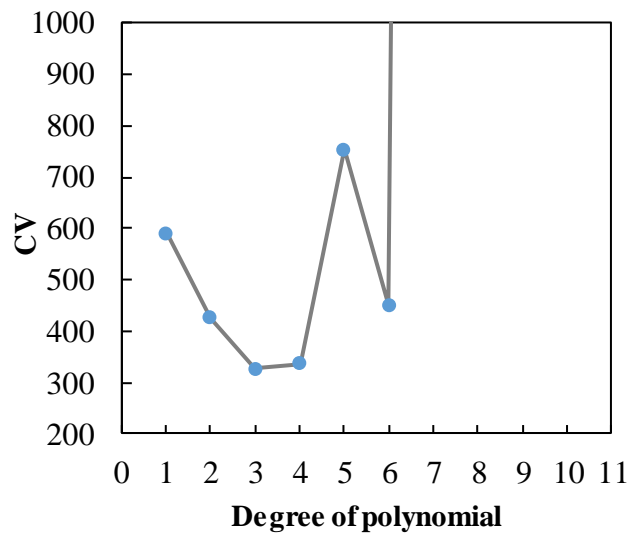


Fig. 3.11 Value of cross-validation by degree of polynomial

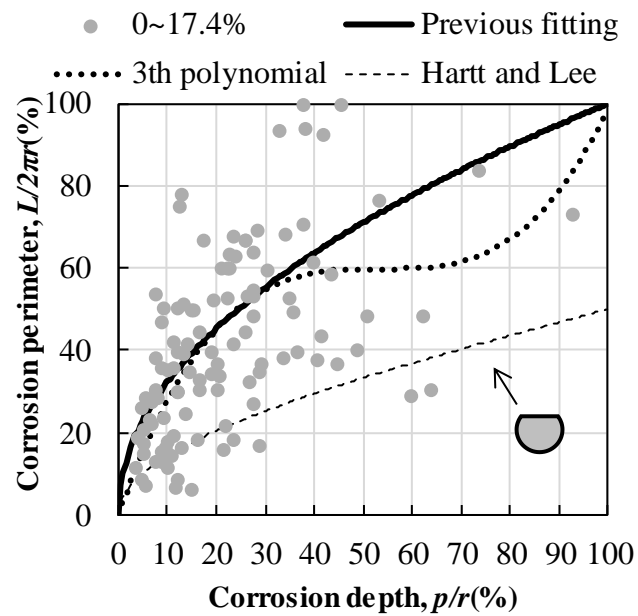


Fig. 3.12 Result of regression with newly determined target range

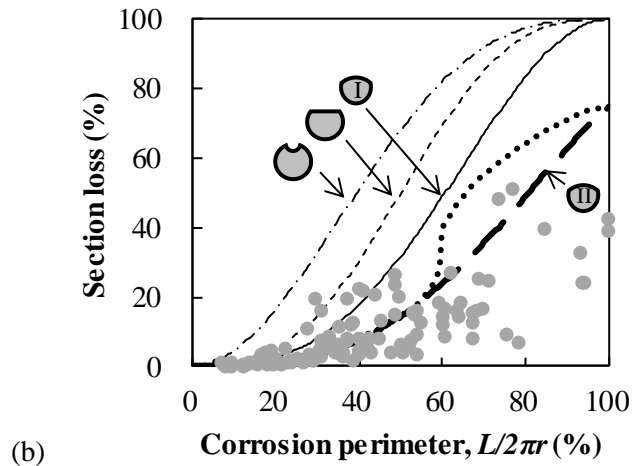
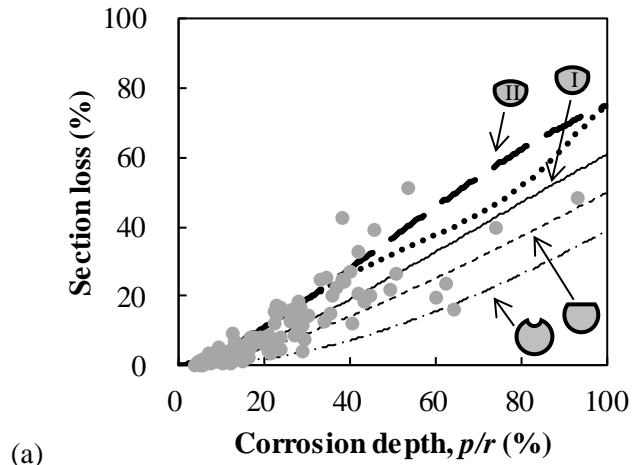
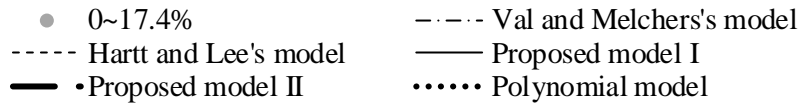


Fig. 3.13 Comparison between measured corroded wire sections and corrosion models: (a) versus corrosion depth; (b) versus corrosion perimeter.

3.3 Corrosion Model of Wires using the Both Corrosion Depth and Corrosion Perimeter

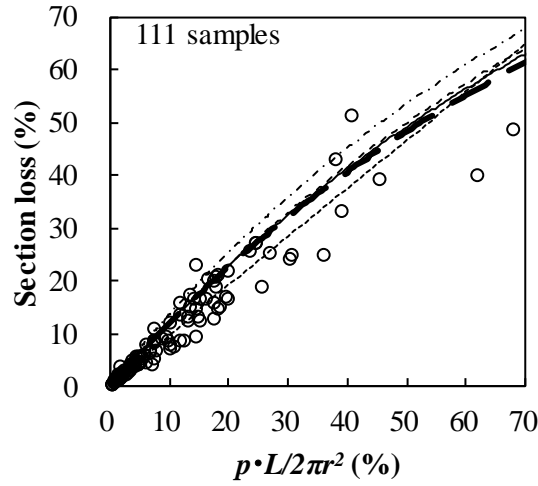
Previous studies (Darmawan and Stewart 2007; Guo et al. 2010; Hartt and Lee 2016; Val and Melchers 1997) has adopted a corrosion model which has only one length parameter, corrosion depth, for estimating the section loss in wire. Likewise, this thesis proposed two corrosion models, Proposed model I and II, which calculate the section loss in wire by only one length parameter, corrosion depth or perimeter. However, the section loss in wire is two dimensional value whereas the length parameter is just one dimensional value. This dimensional difference could limit the accuracy of estimation of section loss in wire. In this aspect, a corrosion model which contains both corrosion depth and perimeter should be developed based on the advantage that both length perimeters of wire samples are measured in this study.

Because the section loss in wire has a unit of area, the section loss in wire is expressed by the product of corrosion depth and perimeter. This concept is basically used in triangle and quadrangle. Fig. 3.14 (a) which presents the section loss in wire versus the product of corrosion depth and perimeter shows a certain tendency. In addition, lines drawn from existing models display a bias with measured values. For identifying the tendency, the graph is plotted in log scale as shown in Fig. 3.14 (b). In log scale, the section loss in wire and the product of corrosion depth and perimeter present a strong linear relationship with 0.95 of correlation coefficient which is very close to 1.0. Thus, it can be concluded that there exists a linear relationship between the section loss in wire and the product of corrosion depth and perimeter. This linear relationship is formulated as:

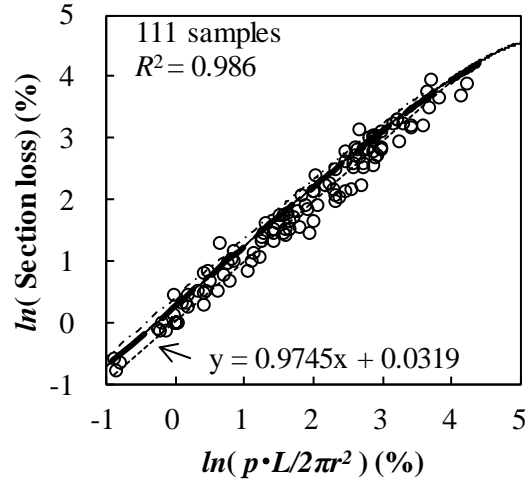
$$\ln\left(\frac{\eta_w}{\pi r^2} \times 100\right) = 0.97 \ln\left(\frac{pL}{2\pi r^2} \times 100\right) + 0.03 \quad (3.19)$$

where η_w is section loss in wire. This formulation is the corrosion model when both corrosion depth and perimeter are known and is called as Proposed model III.

- Measured wire cross-section - - - - - Val and Melchers's model
- - - - - Hartt and Lee's model ——— Proposed model I
- Proposed model II - - - - - Proposed model III



(a)



(b)

Fig. 3.14 Comparison between measured corroded wire sections and corrosion models: (a) section loss versus the product of corrosion depth and corrosion perimeter; and (b) plotting in log scale.

CHAPTER 4

Estimating Corrosion in the 7-wire Steel Strands of External Tendons Using Corrosion Models

The mean corrosion depth and corrosion perimeters in wires and the section loss in strands have a monotonic increasing trend when corrosion in the invisible region is not considered. As an extension of the study conducted by Yoo et al. (2018), estimations of the section loss in corroded strands was performed using a geometric corrosion progress model for wires, and the applicability of the model is discussed here.

Prior to applying the wire corrosion progress models to strands, the limitations of visual inspection must be noted. Measuring either the depth or the perimeter of corrosion in the visible region requires an inspection of the strands from all directions. However, the strands are surrounded by neighboring strands and filling material, which can make access to the corroded strands problematic. Despite these limitations, it was assumed that a corroded strand could be visually inspected from most directions outside of the strand, and that measuring the corrosion depth and perimeter could be conducted without interruption.

4.1 Using Corrosion depth to Estimate Section loss

4.1.1 Results of estimation

The first step in estimation involves measuring the corrosion depth of the visible region for each wire in the strand. Following measurement, the section losses of each wire could be calculated via the aforementioned Proposed model I. Finally, the section loss in a strand was estimated by summing the section losses for each wire. This process was applied to all sampled cross-sections of strands, and the estimated section losses were plotted with respect to the mean corrosion depth, as shown in Fig. 4.1 (a). The x -axis of this figure is mean corrosion depth of visible region in six outer wires. For comparison purpose, actual section loss was also plotted. The mean corrosion depths were determined by averaging measured corrosion depth in visible region. In Fig. 4.1 (b), results of estimating section losses are shown assuming all seven wires are accessible.

Comparison between actual and estimated section losses showed that both section losses are comparable except two strand cross sections. Differences between actual and estimated section losses were ranged from -1.7 to 7.8%. The coefficient of determination (R^2) which represents the adequacy of the estimation was 0.681. If two sections that showed large error are excluded, the R^2 increases to 0.842. For identifying the applicability of this estimation, the causes of small and large differences between the actual and estimated section loss in strands should be investigated. When it was assumed that all seven wires were accessible, differences between actual and estimated section losses were reduced. The range of the difference was from about -1.8% to 4.8%, and the R^2 was increased to 0.851.

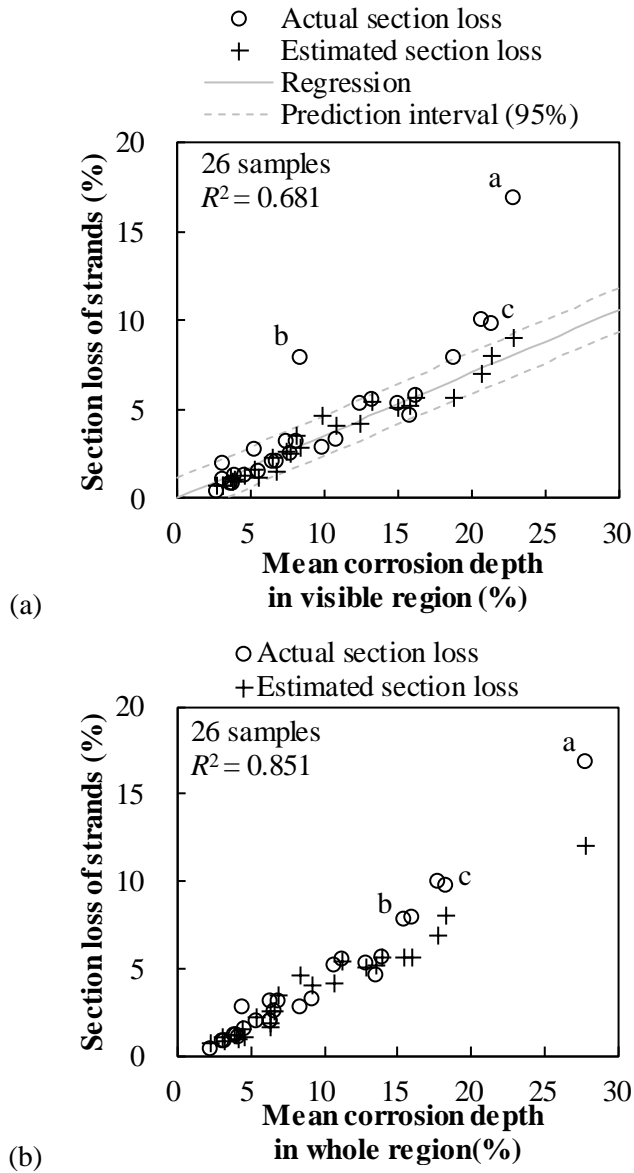


Fig. 4.1 Comparison of actual and estimated section losses for corrosion depth: (a) estimated in visible region; and (b) estimated in whole region

4.1.2 Analysis of Residuals – Section Loss Estimation Using Corrosion Depth

Two factors caused the difference between the actual and the estimated section losses in strands. One was the occurrence of residuals in the corrosion model, and the other was hidden corrosion in invisible regions.

The residual caused by the corrosion model is shown in Fig. 4.2 (a). The figure shows the residual of the estimation when the section loss was estimated for the entire region, so that the effect of the limited visibility could be excluded. Residuals ranged from -1.8 to 4.8%, which was much smaller than the residuals of wires using the same model. According to Yoo et al. (2018), the range of residuals between the actual and the estimated section losses of wires should range from -20 to 28%. The strand residuals were dramatically reduced because the residuals for each wire due to the corrosion model were averaged. Table 4.1 shows the residuals for each wire due to the corrosion model for two strand cross-sections, which are marked as a and c in Fig. 4.1 and Fig. 4.2, respectively. Four wires in the cross-section a were identified as corroded wire. As shown in Fig. 4.3, estimates of the corroded area using the corrosion model were smaller than the actual, and the residuals in each wire ranged from 1.4 to 16.6%. However, since corrosion was not detected in two wires, the residual in the strand cross-section due to the corrosion model was reduced to 4.8%, which was the maximum among the residuals of all strand cross-sections. In cross-section c, corrosion was detected in five wires. Corrosion shapes of the strand cross-sections for each of the wires are shown in Fig. 4.4. The residuals in each wire due to the corrosion model ranged from -10.2 to 8.9%. Due to the negative residual, the strand cross-section residual was only 1.7%.

Due to the limited visibility, estimates of each section loss were smaller than the estimated loss for the entire region because the corrosion depth of the visible

region could only be equal to, or smaller than, the corrosion depth for the entire region. To quantify the estimation of residuals that occurred because of limited visibility, the differences subtracted from the estimates of section loss for the visible region from that of the entire region are plotted as Fig. 4.2 (b). Since corrosion in the invisible region was found in only five strands, the differences amounted mostly to zero. Residuals produced in the sections with limited visibility ranged from 0.2 to 3.0%.

The sum of two estimation residuals is the total estimation residual, as shown in Fig. 4.2 (c). Total residuals were mostly less than 5%, with the exception of two strand cross-sections. The largest of the residuals was about 7.8%, which is designated as a in Fig. 4.1 and Fig. 4.2 and was found in the cross-section with the largest section loss from among the samples. The sizes of the residuals due to the corrosion model and the limited visibility were about 4.8 and 3.0%, respectively. The cross-section of this sample appears in Fig. 4.3 (a) and (b) and shows the actual corrosion shape and the idealized corrosion shape per Proposed model I in the visible region. The corrosion shape of Proposed model I was clearly smaller than the actual shape of four corroded outer wires. A similar situation occurred in the cross-section designated as b in the figure. On the other hand, the total residual of cross-section c showed less residual than either cross-sections a or b, because the invisible region was not corroded.

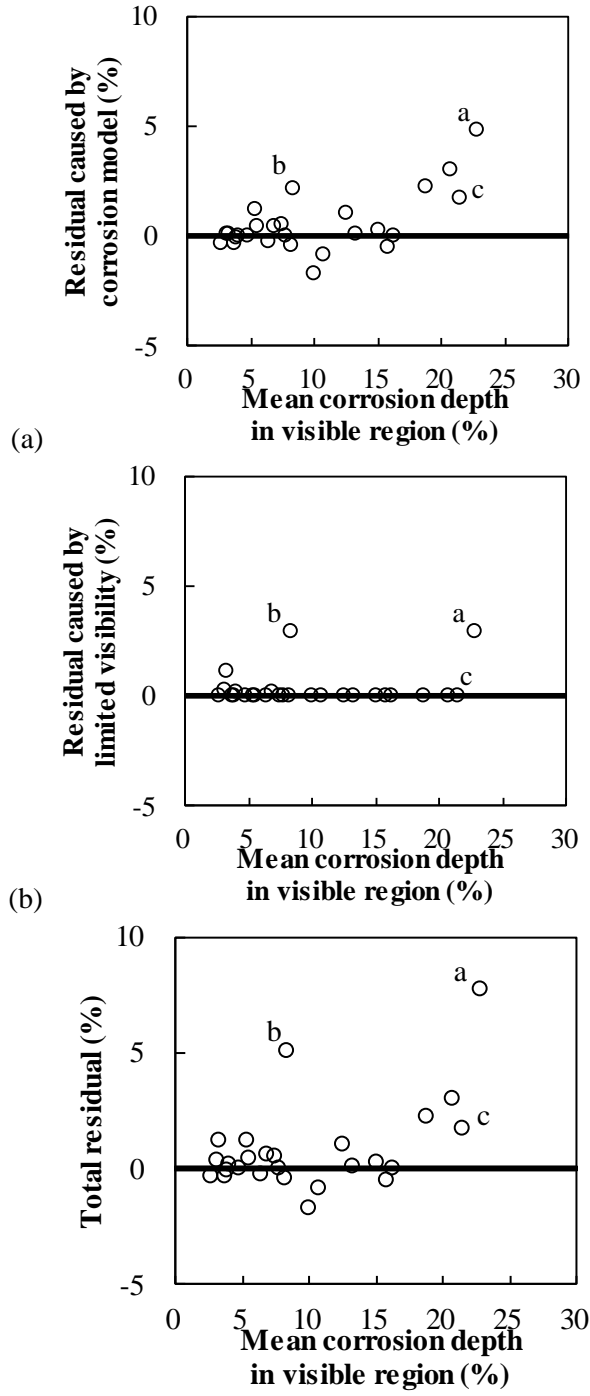


Fig. 4.2 Residuals of section loss: (a) caused by the corrosion model; (b) caused by limited visibility; and (c) total residuals

Table 3.1 Residuals in the Cross-sections of a and c in Fig. 4.1 Due to a Corrosion Model

Cross-section	Residuals in outer wires ^a						Total ^b
	1	2	3	4	5	6	
<i>a</i> in Fig. 4.1	16.6%	13.0%	1.4%	-	-	6.9%	4.8%
<i>c</i> in Fig. 4.1	8.9%	7.7%	-0.1%	-	6.0%	-10.2%	1.7%

^aResiduals were calculated from a corroded area with respect to the nominal cross-sectional area of a wire

^bResiduals were calculated from a corroded area with respect to the nominal cross-sectional area of a strand

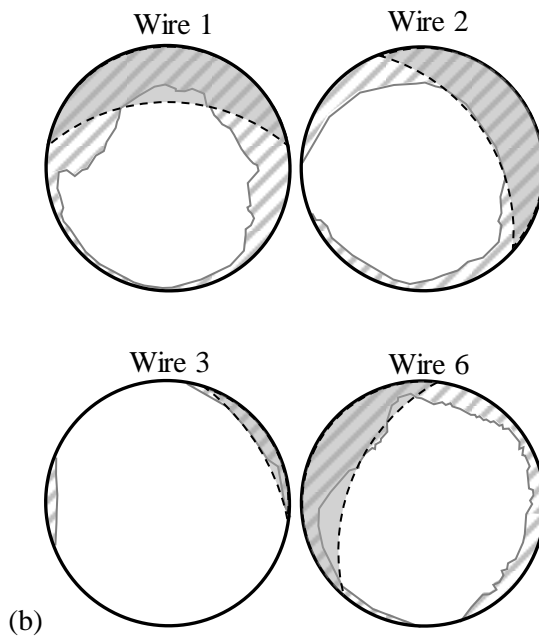
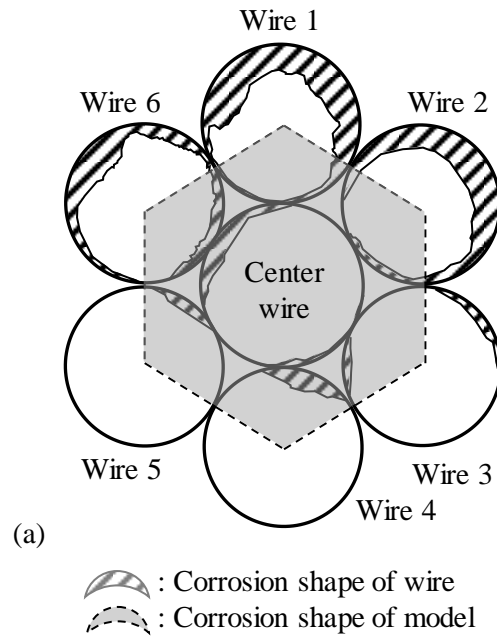
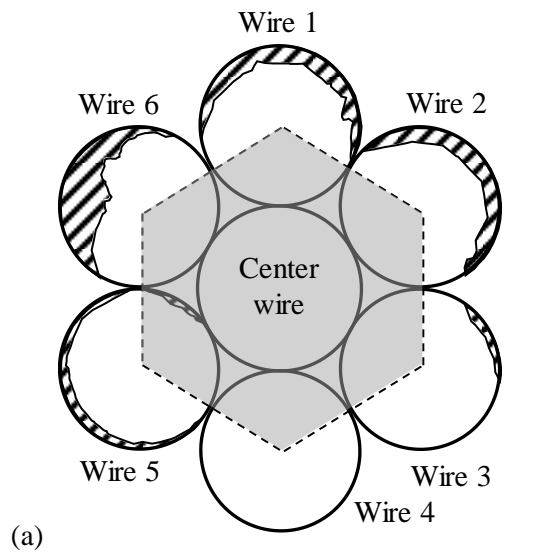


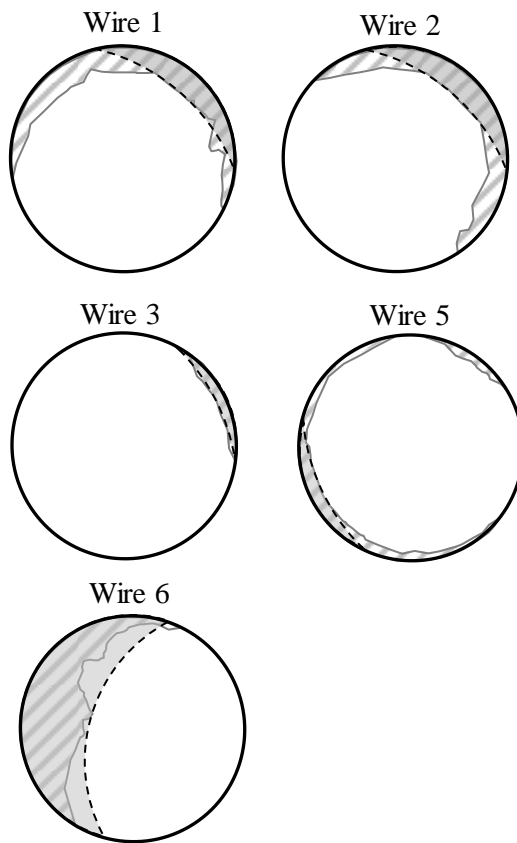


Fig. 4.3 Cross-section *a* in Fig. 4.1 and Fig. 4.2



(a)

 : Actual corrosion shape
 : Estimated corrosion shape per model



(b)

Fig. 4.4 Cross-section c in Fig. 4.1 and Fig. 4.2

4.2 Using Corrosion Perimeter to Estimate Section Loss

4.2.1 Results of estimation

The estimation procedure for section loss in the strands via the use of the corrosion perimeter in the visible region is identical to the use of corrosion depth. The only difference is that Proposed model II is used instead of Proposed model I. The section loss estimated using the measured corrosion perimeter in the visible region is plotted in Fig. 4.5 (a) with respect to the mean corrosion perimeter. The figure shows that the estimated section loss was fairly accurate. The R^2 was 0.646, and the range of residuals was from -6.0 to 5.0%. For comparison, section losses were estimated using the mean corrosion perimeter of the entire region in Fig. 4.5 (b). Since the corrosion perimeters in the invisible regions were considered, the mean corrosion perimeters were significantly increased so that the maximum of the mean was increased to approximately 60%. Estimates of the section loss were almost doubled when the entire region was considered for the cross-section marked as a in the figures. This happened because a significant amount of corrosion was hidden in the invisible region, as shown in Fig. 4.3 (a).

4.2.2 Analysis of Residuals – Section Loss Estimation Using Corrosion Perimeter

Although the reasons for using residuals in estimating section loss are the same for either corrosion perimeter or corrosion depth, the causes are somewhat different. At first, the section loss in strands is estimated by using the corrosion perimeter of the entire region in all seven wires of a strand, as presented in Fig. 4.5 (b), for analyzing the residuals occurring from a wire model. Fig. 4.5 (b) suggests that residual occurrence from a wire model rapidly increases as the mean corrosion perimeter

increases. The residual that occurred from a wire model is presented in Fig. 4.6 (a). The residual ranged from -17.6 to 2.8%. The largest residual was -17.6%, which denotes that the section loss in strands estimated using the corrosion perimeter for an entire region is greater than the actual section loss in strands at 17.6%. These large residuals derive from Proposed model II. The section loss calculated from this model overestimate the actual section loss as the corrosion perimeter increases (Yoo et al. 2018). As Fig. 4.5 (b) shows, the coefficient of determination is a negative value indicating poor correlation. Due to the properties of corrosion progress in wires, compared with corrosion depth, the corrosion perimeter is more restricted by limited visibility. Calculations of the difference in the estimates of section loss between two regions is presented in Fig. 4.6 (b). Limited visibility reduces the estimated section loss in strands by diminishing the corrosion perimeter.

The sum of two residuals, which is the total residual, is plotted in Fig. 4.6 (c). Although the maximum of the residuals from the model and from regions of limited visibility were about -17.6 and 21.0%, respectively, the maximum of the total residual was reduced to -5.0%. This was because the overestimated section loss from the model was compensated for by the underestimated section loss from the invisible region. These results were caused by the properties inherent to the Proposed model II, which conservatively evaluates the section loss in wire by compensating for a large dispersion of the corrosion perimeter. Fig. 4.6 (a) and (b) show several residuals greater than 5 to 10% when the mean corrosion perimeter was greater than 10%, which suggests that estimating section loss by using the corrosion perimeter could be reliable for small corrosion perimeters.

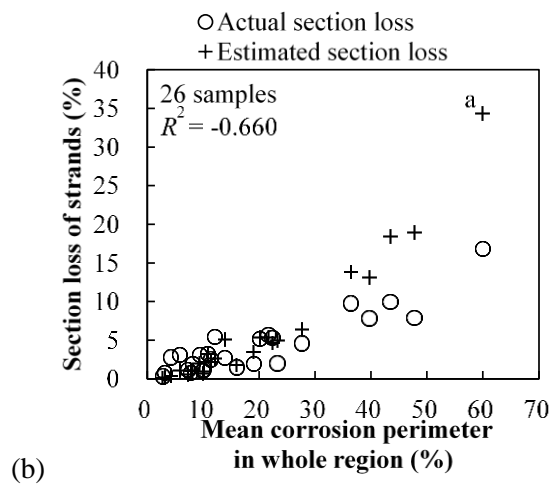
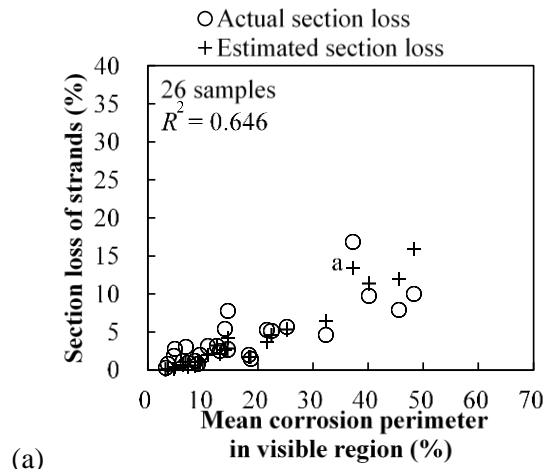


Fig. 4.5 Comparison between actual and estimated section losses for a corrosion perimeter: (a) estimated in the visible region; and (b) estimated in an entire region

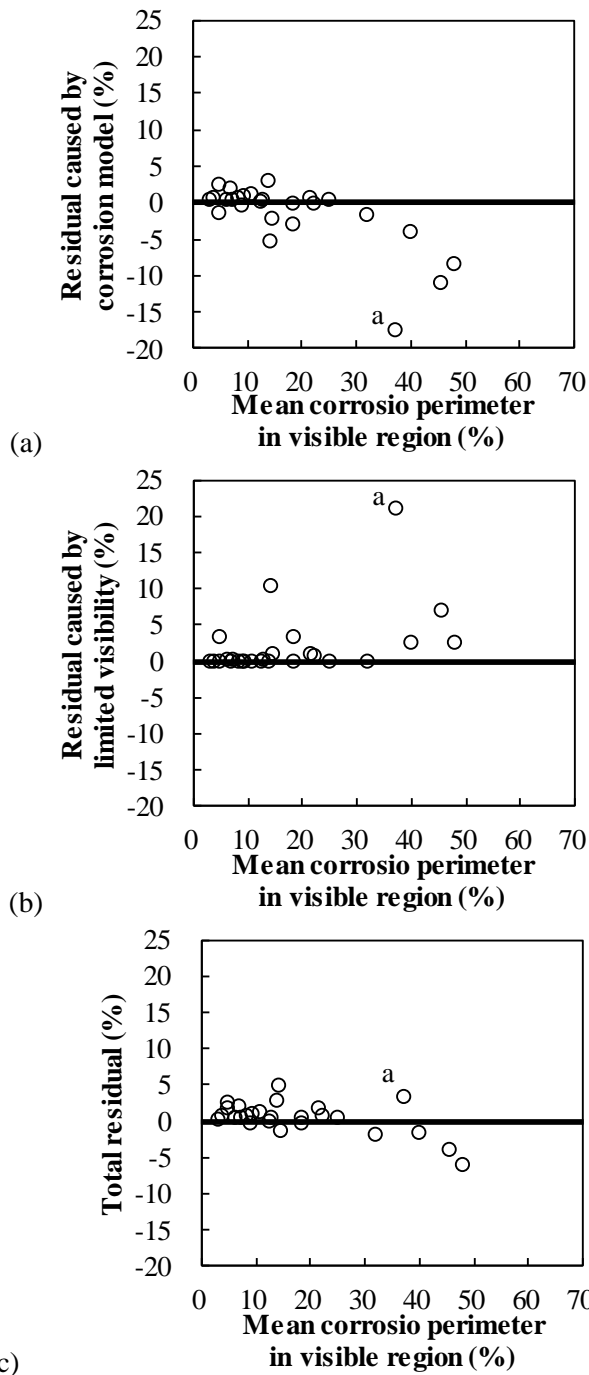


Fig. 4.6 Residuals of section loss: (a) caused by wire model; (b) caused by visual limit; and (c) total residuals

4.3 Using Both Corrosion Depth and Perimeter to Estimate Section Loss

4.3.1 Results of estimation

The section loss in strand is estimated by Proposed model III which uses both corrosion depth and perimeter. Fig. 4.7 (a) presents the estimation result based on the measured corrosion depth and perimeter in the visible region. This graph is plotted with respect to the mean of product of corrosion depth and perimeter in the visible region. As the accuracy of Proposed model III is fairly high, the estimated section loss in strand is highly precise with 0.836 of the R^2 . The residuals which has a range of -0.7 to 5.3% was also smaller than the estimated results by other corrosion models. The estimated result by the corrosion depth and perimeter in whole region is plotted in Fig. 4.7 (b). The R^2 of this result is extremely high value close to 1.0. If the both corrosion depth and perimeter are measurable in whole region, the section loss in strand could be estimated within the error of 3%.

4.3.2 Analysis of Residuals – Section Loss Estimation Using Both Corrosion Depth and Perimeter

Similar to the previous analysis, the residuals caused by the corrosion model and the hidden corrosion in invisible regions are investigated in Fig. 4.8 (a) and (b), respectively. Because of the high accuracy of Proposed model III, the residual caused by the corrosion model has very limited range of -2.4 to 0.8%. On the other hand, the residual caused by visibility limit ranged from 0.0 to 7.6%. Large residual due to visibility limit is produced in two examined cross-sections. These sections

are also problematic to estimate the section loss in strand at chapter 4.1 and 4.2. Unlike the estimation in chapter 4.1 and 4.2, the residual caused by the corrosion model is very small owing to the high accuracy of Proposed model III. However, the residual caused by the visibility limit is still high. Except these sections, the section loss in strand can be estimated within error of 1.5%.

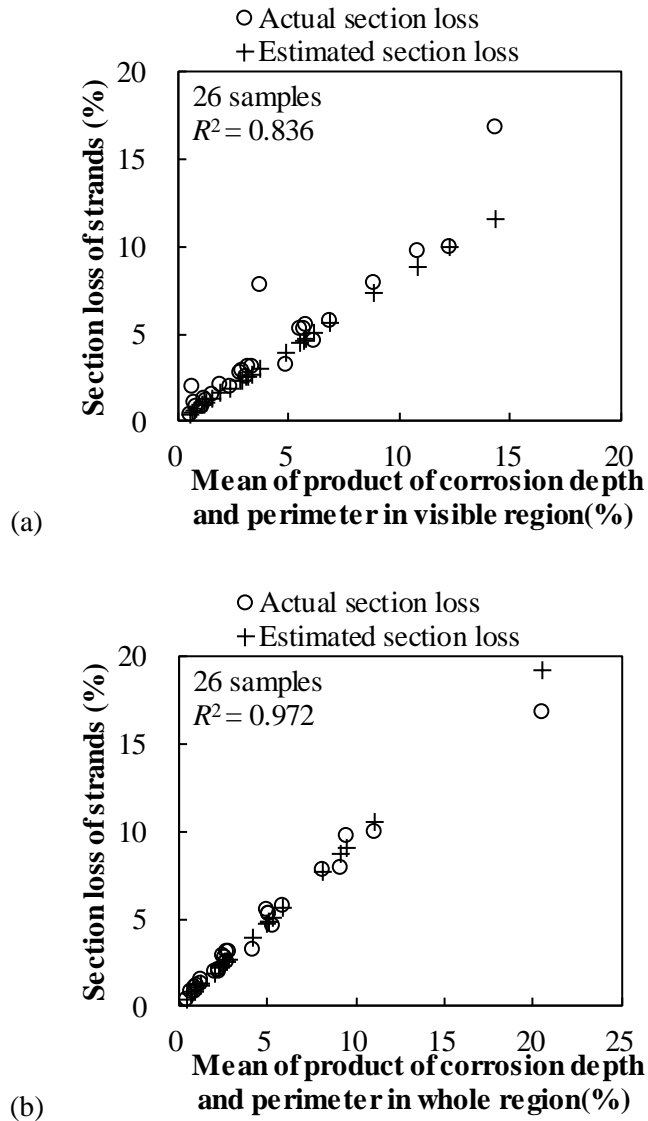


Fig. 4.7 Comparison between actual and estimated section losses for the product of corrosion depth and perimeter: (a) estimated in the visible region; and (b) estimated in an entire region

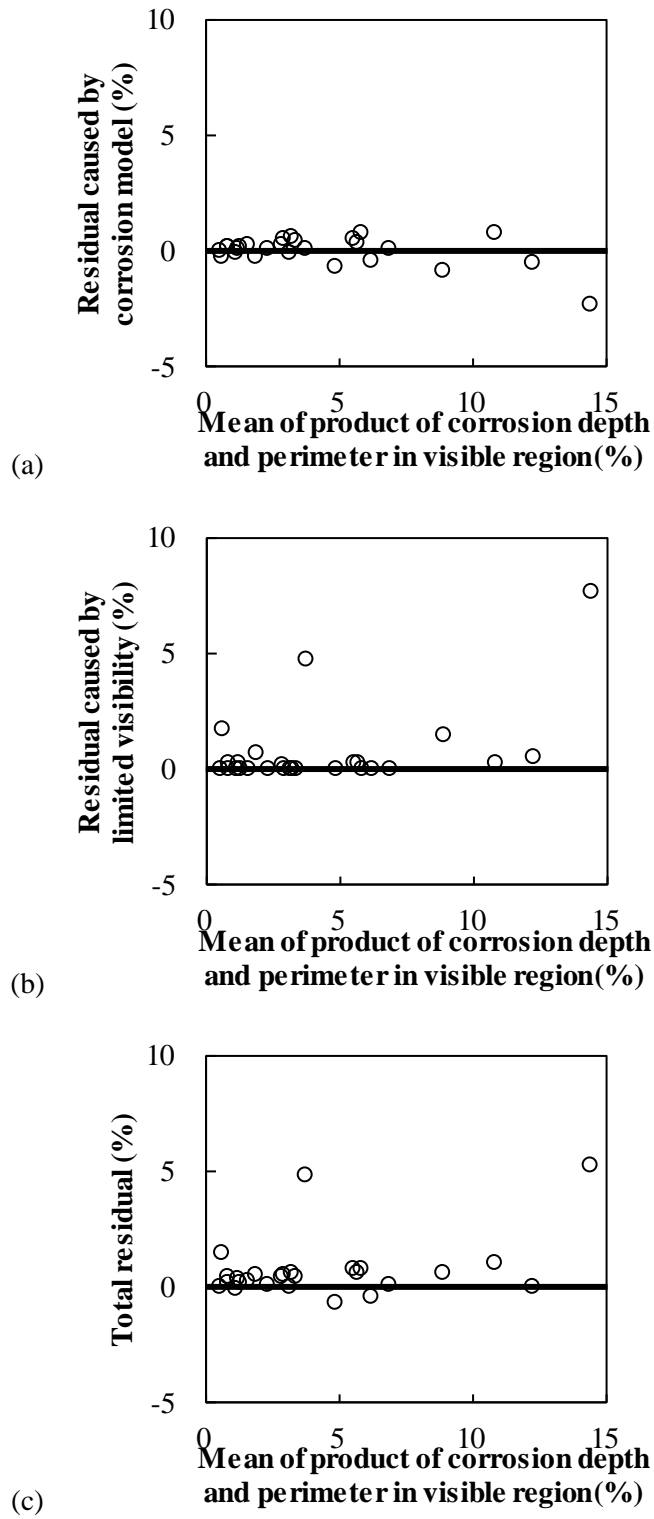


Fig. 4.8 Residuals of section loss: (a) caused by wire model; (b) caused by visual limit; and (c) total residuals

4.4 Evaluating the Remaining Strength of Corroded Strands

The validity of estimating section loss in strands by visual inspection was verified in previous sections. In terms of structural safety, the remaining strength of strands should be evaluated when section loss in a strand has been established via visual inspection.

4.4.1 Strength degradation of corroded strands

Tensile testing is preferable for evaluating the remaining strength of corroded strands. Since the strand samples used in this study were already cut in 120 mm intervals to obtain cross-sections of corroded strands, however, it was not possible to perform tensile testing for these strands. Other studies (Cairns et al. 2005; Du et al. 2005; Jeon et al. 2017; Ma et al. 2013; Stewart 2009), have shown that the remaining strength of a corroded strand is lower than the strength calculated by the remaining cross-section to a certain degree. With the exception of Jeon et al. (2017), all other researchers index the remaining strength of corroded strands with respect to the average section loss by measuring the weight differences before and after corrosion. The average section loss is inappropriate for evaluating the remaining strength, however, because strength should be determined mostly at the section with maximum loss. The research by Jeon et al. (2017) was the only study where the section losses were measured at the fractured cross-section following tensile testing. For this reason, the results of tensile testing by Jeon et al. (2017) are considered the standard for evaluating strength degradation in corroded strands.

Jeon et al. (2017) conducted tensile testing for 14 corroded strands. The strands were obtained from the same bridge as the samples used in the present study. The

ultimate strengths of the corroded strands with respect to the section loss at the fractured cross-section are presented in Fig. 13. The results of the tensile testing showed that the ultimate strength of the corroded strands was reduced as the section loss increased. The mean regression equation for the results is proposed in Eq. (4.1).

$$\frac{F_{uc}}{F_{u0}} \times 100 = 100 - 1.39\eta_s \quad (4.1)$$

where F_{u0} is the nominal ultimate strength of a strand and F_{uc} is the ultimate strength of the corroded strand. Maximum section loss is denoted as η_s (%). The equation indicates that the additional loss in ultimate strength due to corrosion is about 39%. It is presumed that the uneven surface of a corroded area develops stress concentration.

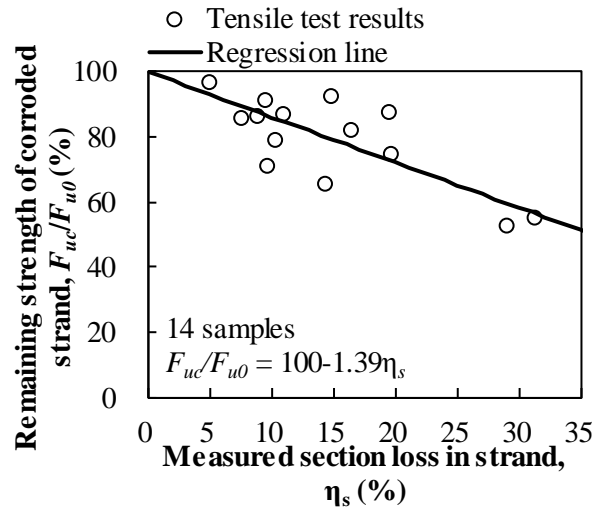


Fig. 4.9 Results of tensile test in Jeon et al. (2017)

4.4.2 Application of Section loss by Using Corrosion Depth for Ultimate Strength Evaluation

The main purpose for estimating section loss is to evaluate the remaining strength of corroded strands. Thus, if corrosion depth is directly related to ultimate strength, an accurate estimate is both practical and paramount. To achieve such a goal, linear regression was conducted to formulate section loss with respect to the corrosion depth. Since estimates for section loss with respect to the mean corrosion depth in the visible region presented in Fig. 4.1 (a) seems to follow a linear trend, regression analysis was performed, and Eq. (4.2) was obtained.

$$\eta_s = 0.353p_s \quad (4.2)$$

In Eq. (4.2), p_s is the mean corrosion depth in the visible region. The results of regression analysis and the prediction intervals of $\pm 95\%$ are plotted in Fig. 4.1 (a). Substituting Eq. (4.2) into Eq. (4.1) derives the relationship between the remaining strength and the corrosion depth as shown in Eq.(4.3).

$$\frac{F_{uc}}{F_{u0}} \times 100 = 100 - 1.39(0.353p_s) = 100 - 0.491p_s \quad (4.3)$$

Fig. 4.10 shows the ultimate strength of the corroded strands with respect to the mean corrosion depth along with the regression results. The prediction intervals of $\pm 95\%$ were also plotted. With the exception of two cross-sections that were considered outliers, the actual section loss fell within $\pm 95\%$ of the predicted interval. In particular, estimation shows good agreement where corrosion depth is small, which could be frequently found in an inspection.

For the purposes of inspection, it is useful to provide a range of corrosion depths indicating the remaining strength of a corroded strand. In taking a conservative approach, the 95% prediction interval of the section loss was applied as the

upper boundary, as shown in Eq. (4.4).

$$\frac{F_{uc}}{F_{u0}} \times 100 = 100 - 1.39(0.353p_s + 1.96\sigma_s) = 98.3 - 0.491p_s \quad (4.4)$$

In equation (4.4), σ_s is the standard deviation of the regression analysis shown in Eq. (4.2). The ranges of the remaining strength in 5% intervals and the corresponding section loss and mean corrosion depths are tabulated in Table 4.1. The results show that mean corrosion depths of 6.9, 17.1, and 27.3% correspond to the remaining ultimate strengths of 95, 90 and 85%, respectively. For practical purposes, these ranges for remaining ultimate strength could be limited by roughly 5, 15, and 25% of the mean corrosion depths, respectively.

Table 4.1 Ranges of Ultimate Strength of Corroded Strands and Corresponding Mean Corrosion Depth

Evaluated remaining ultimate strength	Estimated section loss	Mean corrosion depth
95 ~ 100%	0 ~ 2.2%	0 ~ 6.9%
90 ~ 95%	2.2 ~ 5.8%	6.9 ~ 17.1%
85 ~ 90%	5.8 ~ 9.4%	17.1 ~ 27.3%

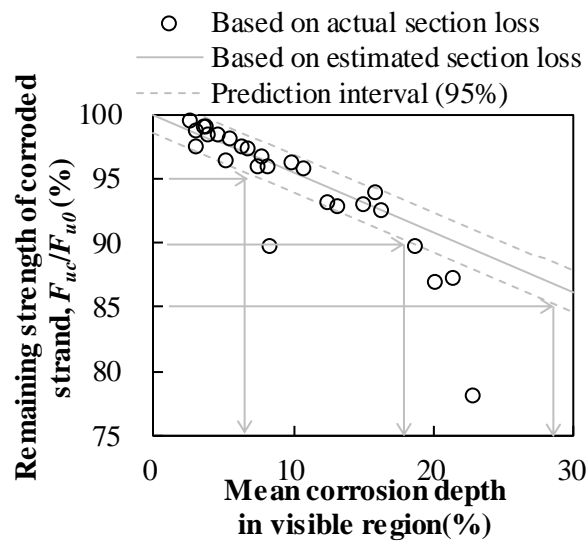


Fig. 4.10 Evaluating the remaining ultimate strength of corroded strands using estimates of section losses

4.4.3 Application of Section loss by Using Corrosion Perimeter for Ultimate Strength Evaluation

Remaining strength could also be evaluated by the estimation of section loss using corrosion perimeter. Fig. 4.11 (a) presents the regression line, which is formulated in Eq. (4.5), between the corrosion perimeter in visible region and the estimated section loss in strand and the prediction intervals of $\pm 95\%$. Because of large variability of estimated section loss in strand by using corrosion perimeter, the result of regression analysis presents broader prediction intervals than those in the case of corrosion depth.

$$\eta_s = 0.258L_s \quad (4.5)$$

L_s is the mean corrosion perimeter in the visible region. The remaining strength via the corrosion perimeter in visible region could be expressed as Eq. (4.6) by substituting Eq. (4.5) into Eq. (4.1) and plotted in Fig. 4.11 (b).

$$\frac{F_{uc}}{F_{u0}} \times 100 = 100 - 1.39(0.258L_s) = 100 - 0.359L_s \quad (4.6)$$

The lower boundary of prediction interval in Fig. 4.11 (b) can be used for estimating the section loss in strand for a conservative way. This is formulated as:

$$\frac{F_{uc}}{F_{u0}} \times 100 = 100 - 1.39(0.258L_s + 1.96\sigma_s) = 95.8 - 0.359L_s$$

The ranges of the remaining strength in 5% intervals and the corresponding section loss and mean corrosion perimeters are tabulated in Table 4.2. The results show that mean corrosion depths of 2.2, 16.2, and 30.1% correspond to the remaining ultimate strengths of 95, 90 and 85%, respectively. For practical purposes, these ranges for remaining ultimate strength could be limited by roughly 2, 15, and 30% of the mean corrosion perimeters, respectively.

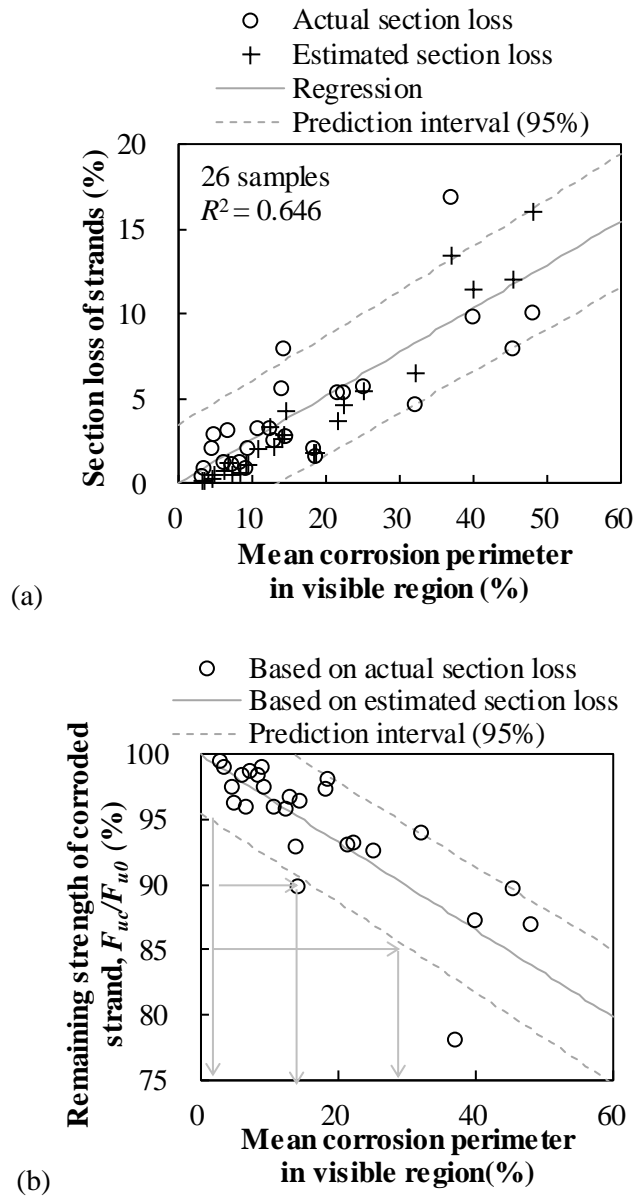


Fig. 4.11 Results of regression analysis: (a) comparison of actual and estimated section losses in visible region; (b) evaluating the remaining ultimate strength of corroded strands using estimates of section losses.

Table 4.2 Ranges of Ultimate Strength of Corroded Strands and Corresponding Mean Corrosion Perimeter

Evaluated remaining ultimate strength	Estimated section loss	Mean corrosion perimeter
95 ~ 100%	0 ~ 2.2%	0 ~ 2.2%
90 ~ 95%	2.2 ~ 5.8%	2.2 ~ 16.2%
85 ~ 90%	5.8 ~ 9.4%	16.2 ~ 30.1%

CHAPTER 5

Estimating Corrosion in the 7-wire Steel Strands of External Tendons Using Monte Carlo Simulation

The estimation method of section loss in strand was validated by restrictive number of the 26 samples. However, various configuration of corrosion such as various location of corrosion, corrosion depth and section loss in wire can be existed. For the extensive validation of the estimation method, more samples should be investigated. At this time, the Monte Carlo simulation can provide a breakthrough.

For performing Monte Carlo Simulation, the probabilistic characteristics of corrosion should be established. Firstly, the concept of middle point of corrosion will be introduced. This point has a role of corrosion initiation which cannot be identified in on-site condition. Secondly, the probabilistic characteristics of corrosion depth and perimeter are established based on the location of the middle point of corrosion. Next, the variability of section loss in wire to corrosion depth and perimeter is defined by using generalized linear model. At last, the corroded strand will be generated while considering the possible occurrence of the number of corroded outer wires.

Based on these probabilistic characteristics, the Monte Carlo Simulation is performed for generating randomly corroded wires and strand. At last, the estimation method of section loss in strand will be examined by generated samples.

5.1 Probabilistic Characteristics of Corrosion in Wires and Strands

5.1.1 Middle point of corrosion

To understand the property of corrosion in strand, it will be helpful to identify the location of corrosion initiation. However, the location of corrosion initiation cannot be identified in collected samples from actual bridge site. Instead, this paper analyzed the middle point of corrosion defined as the half of corrosion perimeter as shown in Fig. 5.1. The middle point of corrosion is expressed as θ which is the angle from top of the wire to the middle point of corrosion. Owing to the symmetry of wire as shown in Fig. 5.1, the angle θ can be expressed as a value of 0° to 180° . Table 5.1 is the distribution of middle point of corrosion based on 81 corroded wire samples except for the four center wire samples in 85 corroded wire samples. Total frequency of middle point of corrosion is larger than the number of investigated wire samples because some wire samples like Fig. 2.11 (d) have two or more middle points of corrosion in one wire. As shown in Table 5.1, total 23.1% of middle point of corrosion occurs in invisible region.

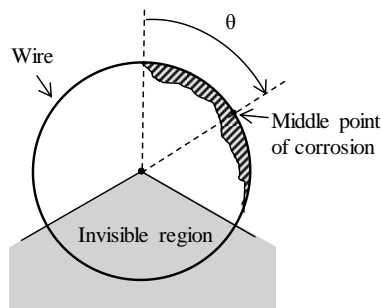


Fig. 5.1 Middle point of corrosion

Table 5.1 Frequencies of the middle point of corrosion

Interval	Frequencies, EA	Frequencies (%)
0° ~ 30°	42	38.9 %
30° ~ 60°	18	16.7 %
60° ~ 90°	16	14.8 %
90° ~ 120°	7	6.5 %
120° ~ 150° (invisible region)	5	4.6 %
150° ~ 180° (invisible region)	20	18.5 %
Total	108	100 %

5.1.2 Corrosion depth and perimeter by the location of middle point of corrosion

In one wire, the corrosion characteristics will be different depending on the location. The wire in visible region will occur more corrosion than the wire in invisible region as listed in Table 5.1 because the wire in visible region has more chance to be exposed to corrosion inducers. For the same reason, the corrosion degree and occurrence will be severe in the upper region of wire than the lower region of wire. The best way to investigate these characteristics is checking the corrosion depth and perimeter with corrosion initiation point. However, the corrosion initiation point cannot be identified. In this point, the corrosion depth and perimeter with the middle point of corrosion are investigated. The mean and standard deviation (Std.) of corrosion depth and perimeter by the angle of the middle point of corrosion are summarized in Table 5.2.

The mean corrosion depth and perimeter tend to get smaller as the angle of the middle point of corrosion gets larger. The smallest mean corrosion depth is occurred in invisible region while the mean corrosion perimeter is occurred in visible

region. This infers the corrosion shape in invisible region as a thin and long shape. The standard deviation in visible region tends to be larger than that in invisible region. This can be inferred from the standard deviations that the visible region is exposed to various corrosive environment whereas the invisible region may be exposed to similar environment because of the protective condition.

Table 5.2 The mean and standard deviation of corrosion depth and perimeter by the angle of the middle point of corrosion

Interval	Frequencies, EA	Corrosion depth (%), p/r		Corrosion perimeter (%), $L/2\pi r$	
		Mean	Std.	Mean	Std.
$0^\circ \sim 30^\circ$	42	23.2	6.07	41.8	67.8
$30^\circ \sim 60^\circ$	18	19.0	2.07	34.0	59.2
$60^\circ \sim 90^\circ$	16	10.1	0.65	15.8	13.1
$90^\circ \sim 120^\circ$	7	11.8	1.98	13.5	3.39
$120^\circ \sim 150^\circ$	5	6.35	0.14	22.7	13.9
$150^\circ \sim 180^\circ$	20	7.68	0.56	16.9	14.8

* Bolded interval means invisible region.

5.1.3 Probability distribution of corrosion depth and perimeter

To carry out Monte Carlo Simulation, not only the mean and standard deviation of variable but also the probability distribution is essential. In the literature, the probability distribution of corrosion depth was used as Lognormal (Sheikh et al. 1990) and Gumbel distribution (Darmawan and Stewart 2007) while there is no literature related with the corrosion perimeter.

For estimating the probability distribution of corrosion depth and perimeter, da-

ta is fitted to eight probability distributions (Normal, Lognormal, Gumbel, Beta, Weibull, Rayleigh, Exponential, Gamma) as listed in Table 5.3. The parameters of probability distributions are estimated by maximum likelihood estimation given in *Matlab* R2017a. To determine the most suitable probability distribution, the goodness of fit is calculated by the Kolmogorov-Smirnov test (K-S test), Akaike information criterion (AIC) and Bayesian information criterion (BIC). K-S test defines the goodness of fit as the maximum distance between the empirical distribution and the assumed distribution. AIC and BIC offer a relative measure of assumed distribution for a given set of data based on likelihood. Goodness of fit of K-S test, AIC and BIC are calculated by Eq. (5.1) to (5.3), respectively.

$$KS = \max_i \left| F(x_i) - \frac{i}{n} \right| \quad (5.1)$$

$$AIC = 2k - 2 \ln(L) \quad (5.2)$$

$$BIC = \ln(n)k - 2 \ln(L) \quad (5.3)$$

where $F(-)$ is cumulative distribution function, x is data point, i is the rank of data point in ascending order, n is sample size, k is number of parameters used in distribution, L is maximized value of likelihood function of model.

Table 5.3 Probability density function of examined probability distributions

Distribution	Parameter	Probability Density Function
Normal	μ, σ	$f(x) = \frac{1}{\sqrt{2\pi\sigma^2}} e^{-\frac{(x-\mu)^2}{2\sigma^2}}$
Lognormal	μ, σ	$f(x) = \frac{1}{x\sqrt{2\pi\sigma^2}} e^{-\frac{(\ln x - \mu)^2}{2\sigma^2}}; x \geq 0$
Gumbel	u, α	$f(x) = \exp(-e^{-\alpha(x-u)})$
Beta	q, r	$f(x) = \frac{1}{B(q, r)} \frac{(x-a)^{q-1} (b-x)^{r-1}}{(b-a)^{q+r-1}}; a \leq x \leq b$
Weibull	k, w	$f(x) = \frac{k}{w-\varepsilon} \left(\frac{x-\varepsilon}{w-\varepsilon} \right)^{k-1} e^{-\left(\frac{x-\varepsilon}{w-\varepsilon} \right)^k}; x \geq \varepsilon$
Rayleigh	α	$f(x) = \frac{x}{\alpha^2} \exp \left[-\frac{1}{2} \left(\frac{x}{\alpha} \right)^2 \right]$
Exponential	λ	$f(x) = \lambda e^{-\lambda x}; x \geq 0$
Gamma	ν, k	$f(x) = \frac{\nu(\nu x)^{k-1}}{\Gamma(k)} e^{-\nu x}; x \geq 0$

The distribution which gives the minimum value calculated from these equations is the most suitable distribution among eight distribution because the lowest value means the closest distribution in K-S test and the distribution of maximum likelihood in AIC and BIC. The goodness of fit of eight distributions are calculated for the corrosion depth and perimeter in each interval. The most suitable distribution of each goodness of fit method is summarized in Table 5.4 and Table 5.5. The Rayleigh distribution which appears most frequently in tables is selected as the probability distribution of corrosion depth and perimeter. The parameter α utilized in Rayleigh distribution via corrosion depth and perimeter for each interval is summarized in Table 5.6.

Table 5.4 The most suitable distribution obtained from K-S test, AIC and BIC via corrosion depth

Interval	Corrosion depth		
	K-S test	AIC	BIC
0° ~ 30°	Beta	Beta	Beta
30° ~ 60°	Normal	Rayleigh	Rayleigh
60° ~ 90°	Gumbel	Rayleigh	Rayleigh
90° ~ 120°	Exponential	Lognormal	Exponential
120°~150°	Rayleigh	Rayleigh	Rayleigh
150°~180°	Lognormal	Lognormal	Lognormal

Table 5.5 The most suitable distribution obtained from K-S test, AIC and BIC via corrosion perimeter

Interval	Corrosion perimeter		
	K-S test	AIC	BIC
0° ~ 30°	Normal	Beta	Rayleigh
30° ~ 60°	Gumbel	Gumbel	Rayleigh
60° ~ 90°	Gamma	Rayleigh	Rayleigh
90° ~ 120°	Lognormal	Lognormal	Rayleigh
120°~150°	Rayleigh	Rayleigh	Rayleigh
150°~180°	Lognormal	Rayleigh	Rayleigh

Table 5.6 Parameter of Rayleigh distribution via corrosion depth and perimeter for each interval

Interval	Corrosion depth	Corrosion perimeter
0° ~ 30°	0.580	6.570
30° ~ 60°	0.474	5.346
60° ~ 90°	0.252	2.486
90° ~ 120°	0.295	2.125
120°~150°	0.159	3.566
150°~180°	0.192	2.661

5.1.4 Section loss in wires via corrosion depth and perimeter

The corrosion depth and perimeter could be generated based on probabilistic characteristics derived in the previous chapter. The section loss in wire can be calculated from the corrosion-model of wire such as Proposed model I and II. However, the section loss of measured wire shows some variability around the section loss obtained from the model as shown in Fig. 3.2 and Fig. 3.5. For a better simulation of the section loss in wire, this variability should be included during the calculation of section loss in wire from the corrosion depth and perimeter.

In order to include the variability, the linear regression could be applied by modeling the relationship between the corrosion depth/perimeter and the section loss in wire. By this simple method, the variability of section loss in wire could be simulated. However, the linear regression cannot be applied in this case because it violates one of the assumption adopted in linear regression. Linear regression assumes the normally distributed residual with zero mean and constant standard deviation whereas the standard deviation of residual obtained from data increases as

the corrosion depth and perimeter grow as can be seen in Fig. 3.2 and Fig. 3.5. In addition, the confidence and prediction intervals contain the negative value while the section loss which has a role of response variable must be always positive value. In this case, the generalized linear model (GLM) which is more generalized method than the linear regression can be an alternative.

GLM proposed by Nelder and Wedderburn (1972) is an extension of linear model by allowing the response variable to have a restricted range such as bounded and binary variable and a non-normal distribution of residuals. GLM is composed of three components, random component, linear predictor, and link function (Fox 2015). A random component specifies the probability distribution of the response variable, Y_i , from the exponential family, such as the Gaussian, binomial, Poisson, gamma, beta, or inverse-Gaussian distribution. A linear predictor, η_i , is a linear combination of unknown parameters, β_i , and explanatory variables x_i .

$$\eta_i = \beta_0 + \beta_1 x_{i1} + \beta_2 x_{i2} + \dots + \beta_k x_{ik} \quad (5.4)$$

A link function $g(-)$ describes the relationship between the expectation of the response variable, $\mu_i = E(Y_i)$, and the linear predictor as follows:

$$g(\mu_i) = \eta_i = \beta_0 + \beta_1 x_{i1} + \beta_2 x_{i2} + \dots + \beta_k x_{ik} \quad (5.5)$$

The common link functions are summarized in Table 5.7. It can be noticed that the linear regression is one of GLM which utilizes the Gaussian distribution of response variable with identify link function.

Table 5.7 Common link functions

Link	$\eta_i = g(\mu_i)$
Identity	μ_i
Log	$\log_e \mu_i$
Inverse	μ_i^{-1}
Logit	$\log_e \frac{\mu_i}{1 - \mu_i}$
Probit	$\Phi^{-1}(\mu_i)$

For applying the GLM, aforementioned three components are required. Firstly, the random component which corresponds to the probability distribution of the section loss in wire should be identified. Since the random component is a continuous variable, there are 4 candidates of probability distribution, Gaussian, gamma, beta, and inverse-Gaussian. The goodness of fit of K-S test, AIC, and BIC are calculated. All three goodness of fit indicate that the gamma distribution is the most suitable distribution for the section loss in wire as shown in Table 5.8. The GLM with gamma distribution is also called as gamma regression.

Secondly, the link function should be determined. The GLM with the exponential families has a canonical link function which makes $g(\mu_i)$ equal to Y_i . The canonical link function of each exponential families is summarized in Table 5.9. Although the canonical link function of gamma distribution is an inverse link, the link function is determined as the log link because the inverse link can produce negative prediction values (Hattab 2016).

Lastly, the regression coefficients are calculated from the regression equation. The regression equation has a form of polynomial form as written in Eq. (5.6) with the inequality constraint of Eq. (5.7). The inequality constraint guarantees that the

section loss in wire gradually increases as corrosion depth or perimeter increases.

$$\text{Regression model : } y = b_0 + b_1x + \cdots + b_nx^n \quad (5.6)$$

$$\text{Inequality constraint : } \frac{dy}{dx} = b_1 + 2b_2x + \cdots + nb_nx^{n-1} \geq 0 \quad (5.7)$$

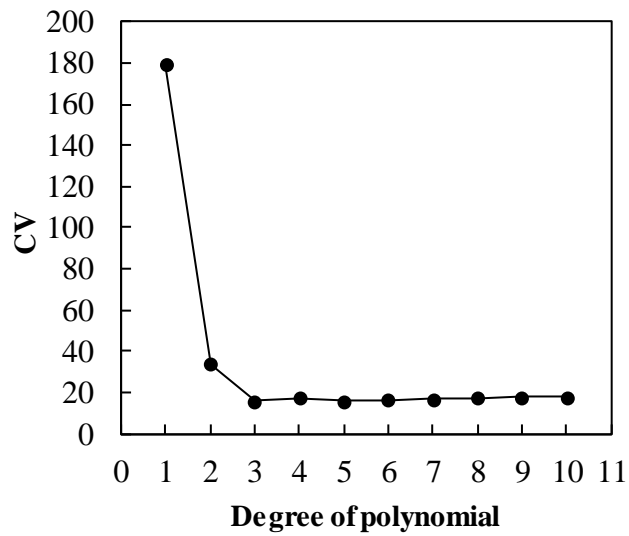
where b_i is regression coefficient. The degree of polynomial for corrosion depth and perimeter are determined as the third and the second degree polynomial by cross-validation as shown in Fig. 5.2 (a) and (b), respectively. The regression coefficients are summarized in Table 5.10. The results of GLM for corrosion depth and perimeter are shown in Fig. 5.3. The prediction interval of gamma regression derived from Hattab (2016) is also illustrated in Fig. 5.3.

Table 5.8 Rank of goodness of fit as a distribution of the section loss in wire

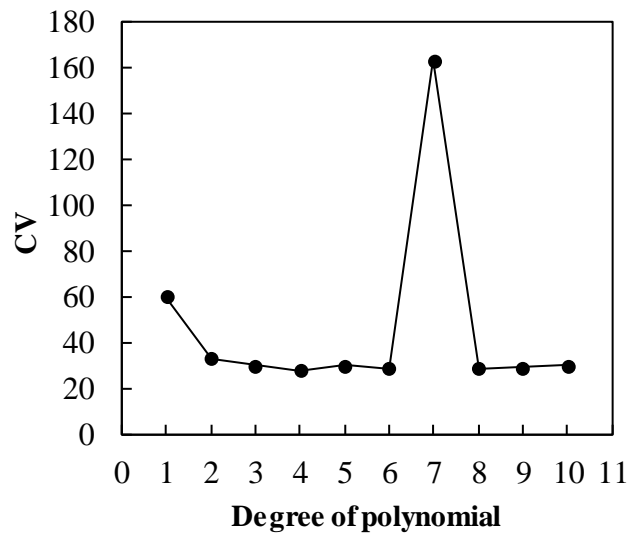
Rank	K-S test	AIC	BIC
1	Gamma	Gamma	Gamma
2	Beta	Beta	Beta
3	Inverse Gaussian	Inverse Gaussian	Inverse Gaussian
4	Gaussian	Gaussian	Gaussian

Table 5.9 Canonical link function for each exponential families

Family	Canonical Link
Gaussian	Identity
Binomial	Logit
Poisson	Log
Gamma	Inverse
Inverse-Gaussian	Inverse-square



(a)

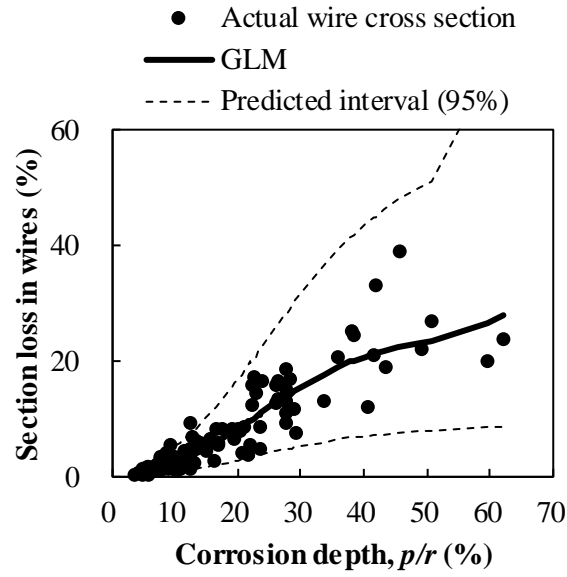


(b)

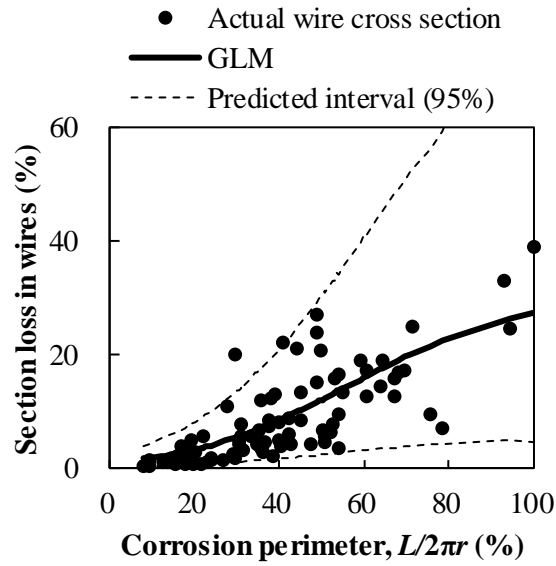
Fig. 5.2 Value of cross-validation by degree of polynomial: (a) corrosion depth; and (b) corrosion perimeter.

Table 5.10 Regression coefficient obtained from GLM

	Regression coefficients			
	b_0	b_1	b_2	b_3
Corrosion depth	-0.87	0.22	-0.0043	0.000029
Corrosion perimeter	-0.50	0.076	-0.00037	-



(a)



(b)

Fig. 5.3 The results of GLM: (a) for corrosion depth; and (b) for corrosion perimeter.

5.2 Generation of Corroded Strands

5.2.1 Generation procedure

Monte Carlo simulation (MCS) is conducted for generating corroded strand according to the flowchart illustrated in Fig. 5.4. First step of the MCS is the generation of the middle point of corrosion. The middle point of corrosion has a role of defining the location of corrosion and is distributed as Table 5.1. The corrosion depth and perimeter of wire are produced in accordance with the location of the middle point of corrosion as summarized in Table 5.2, Table 5.4, and Table 5.5. The section loss in wire will be generated by the results of GLM and its prediction intervals as shown in Fig. 5.3. Until this step, the corroded wires are generated. At last, the corroded wires are allocated to the strand. The number of corroded wires in the allocated strand follows the number of corroded outer wires in investigated strand samples as listed in Table 5.11. At last, the procedure of generating the corroded strands is completed.

Table 5.11 Number of strands sorted by number of corroded outer wires

No. of corroded outer wires	No. of strands
1	4 EA (15.4%)
2	9 EA (34.6%)
3	2 EA (7.7%)
4	4 EA (15.4%)
5	5 EA (19.2%)
6	2 EA (7.7%)
Total	26 EA (100 %)

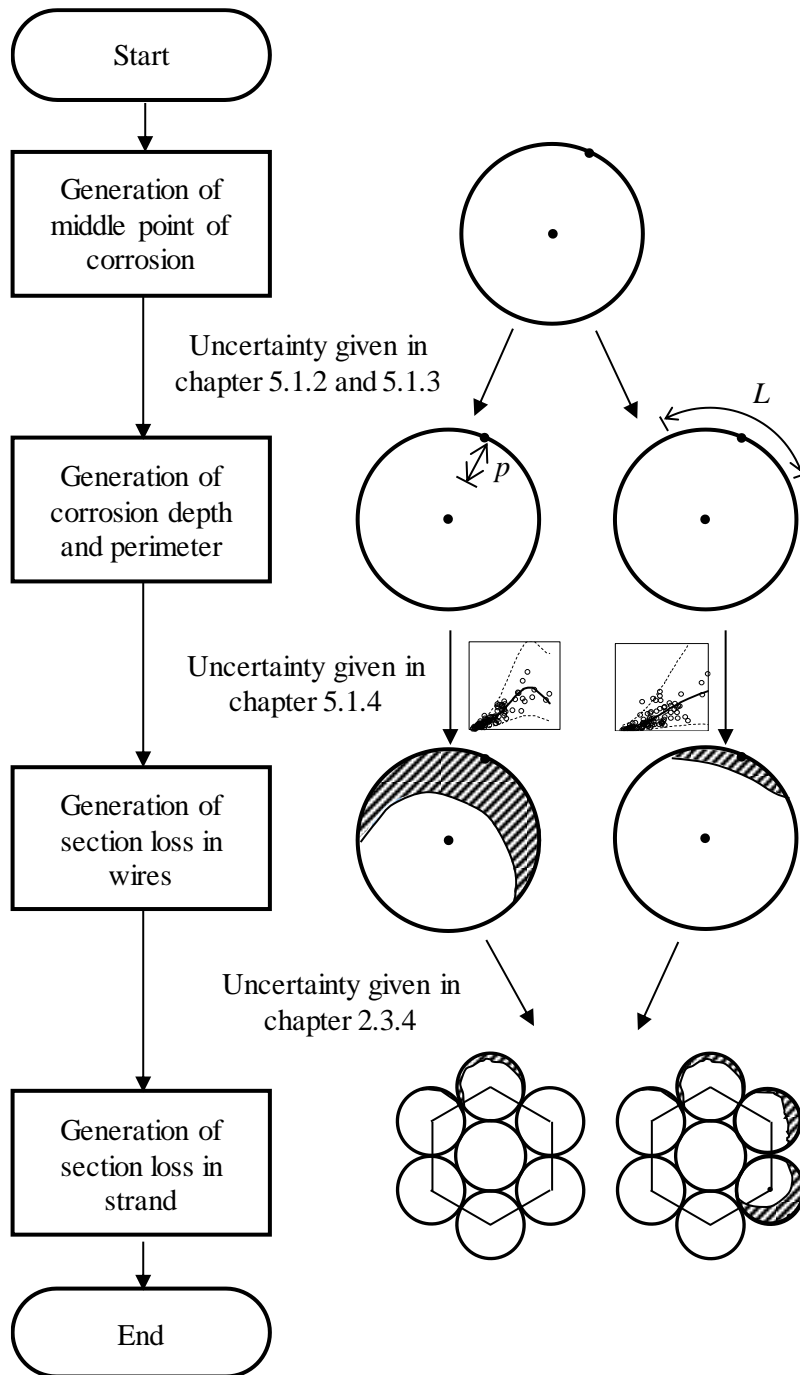


Fig. 5.4 Flowchart of generating the corroded strands

5.2.2 Generation of corroded wires and strands

Total 1,000 corroded wires and strands are generated and represented in Fig. 5.5 and Fig. 5.6, respectively. It can be noticed that the generated cross sections show a comparable result with the measured data presented as a solid circle.

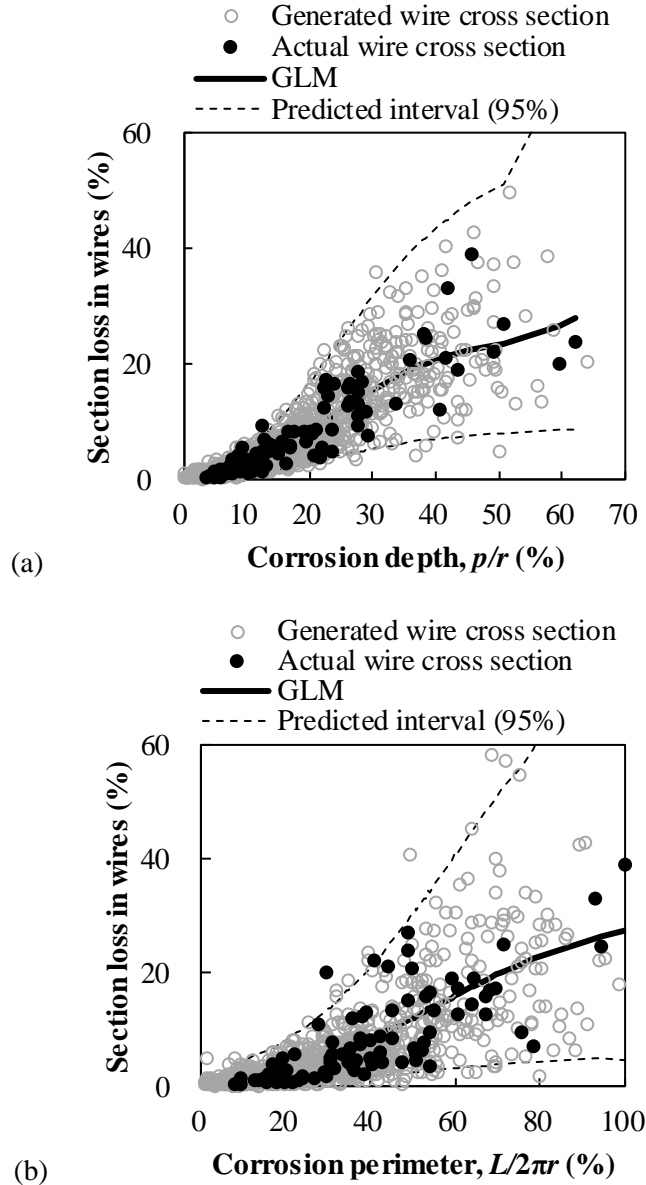
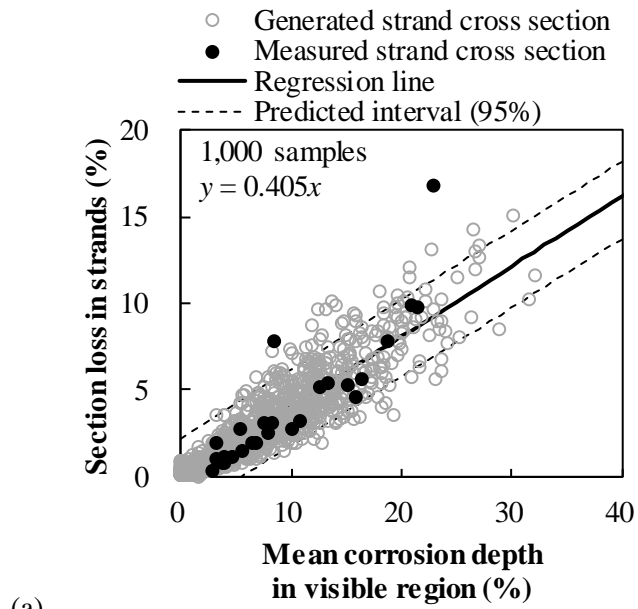
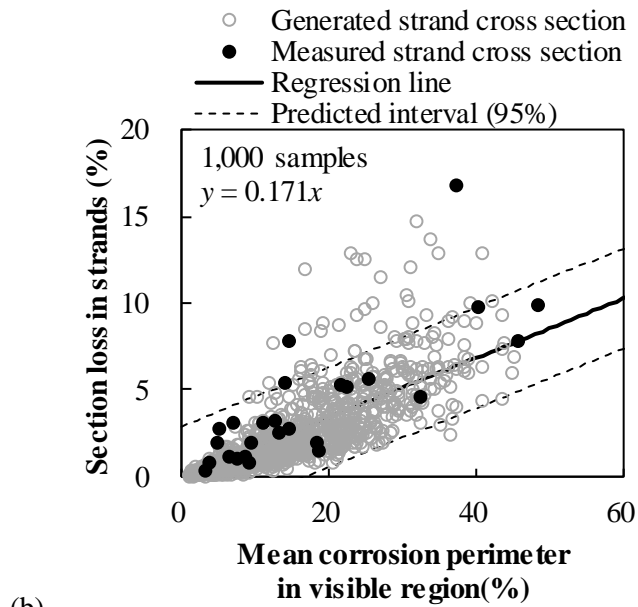


Fig. 5.5 Results of generation in terms of wires: (a) corrosion depth; and (b) corrosion perimeter



(a)



(b)

Fig. 5.6 Results of generation in terms of strands

5.2.3 Discussion of generated result

Generated corroded strands seem to be similar with the measured strands. For the detailed analysis, the regression analysis is performed to both generated and measured data as illustrated in Fig. 5.6, Fig. 5.7 and Fig. 5.8.

Firstly, the analysis result in terms of corrosion depth will be examined. By comparing the results of regression in Fig. 5.6 (a) and Fig. 5.7 (a), it can be noted that the slope of regression is similar in both measured and generated strand whereas the prediction interval of measured strands is broader than that of generated strand. This difference indicates that MCS procedure cannot reflect all uncertainties occurred in reality.

In fact, the prediction interval of measured strands gets broader by the two cross sections designated as a and b in Fig. 5.7 (a). These two cross sections as illustrated in Fig. 2.11 (d) and (e) have a common feature that contains the severe corrosion in invisible region. This feature induces gross section loss against the corrosion depth in visible region. The reason of this asymptomatic corrosion comes from the correlated corrosion between the wires. This correlation includes both the size and location of corrosion because each wire can share the corrosion environment. Fig. 2.11 (a) ~ (e) illustrate the strand cross-sections which have an asymptomatic corrosion. This figure indicate that there would be several wires which contain an asymptomatic corrosion if there is an one wire which contains an asymptomatic corrosion. Because this correlation is not considered in MCS, the prediction intervals of measured and generated strands show a difference. The figure is re-plotted with excluding the asymptomatic corrosion in Fig. 5.7 (b). It can be noticed that the prediction intervals in measured and generated strands has a comparable value.

This correlation effect also appears in the case of corrosion perimeter as can be seen in Fig. 5.6 (b) and Fig. 5.8 (a). The prediction interval in figure re-plotted by excluding the asymptomatic corrosion as presented in Fig. 5.8 (b) is a closer value to the prediction interval in Fig. 5.6 (b) than that in Fig. 5.8 (a).

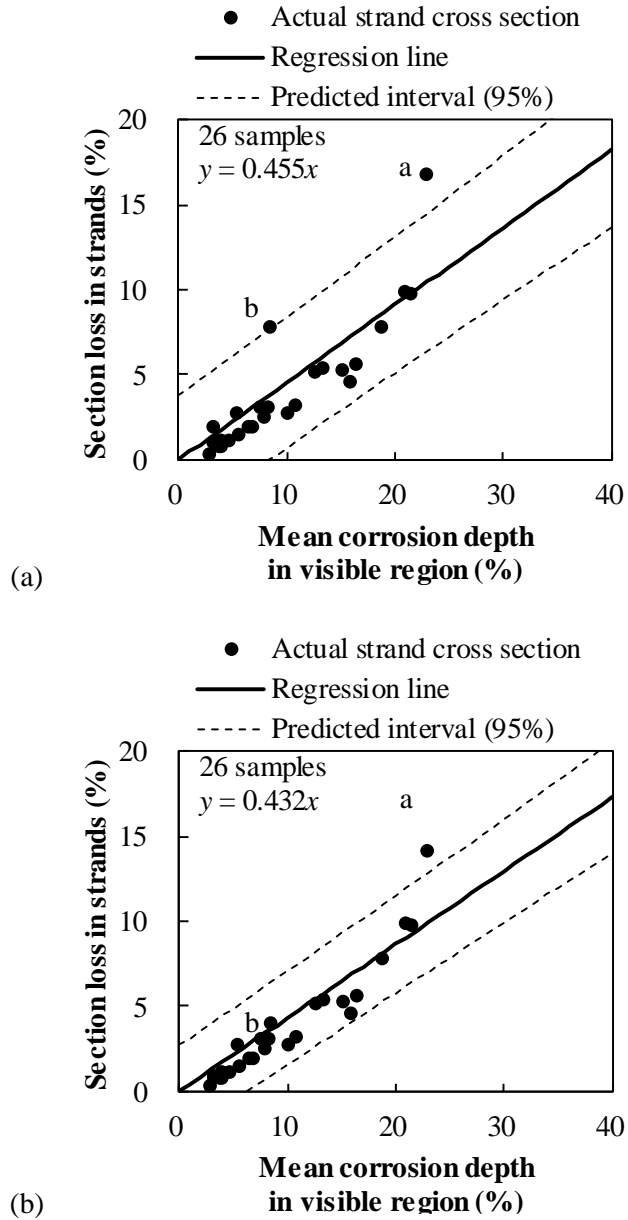


Fig. 5.7 Regression analysis for measured strand cross section with respect to mean corrosion perimeter: (a) considering all of wires; and (b) excluding wires which have an asymptomatic corrosion.

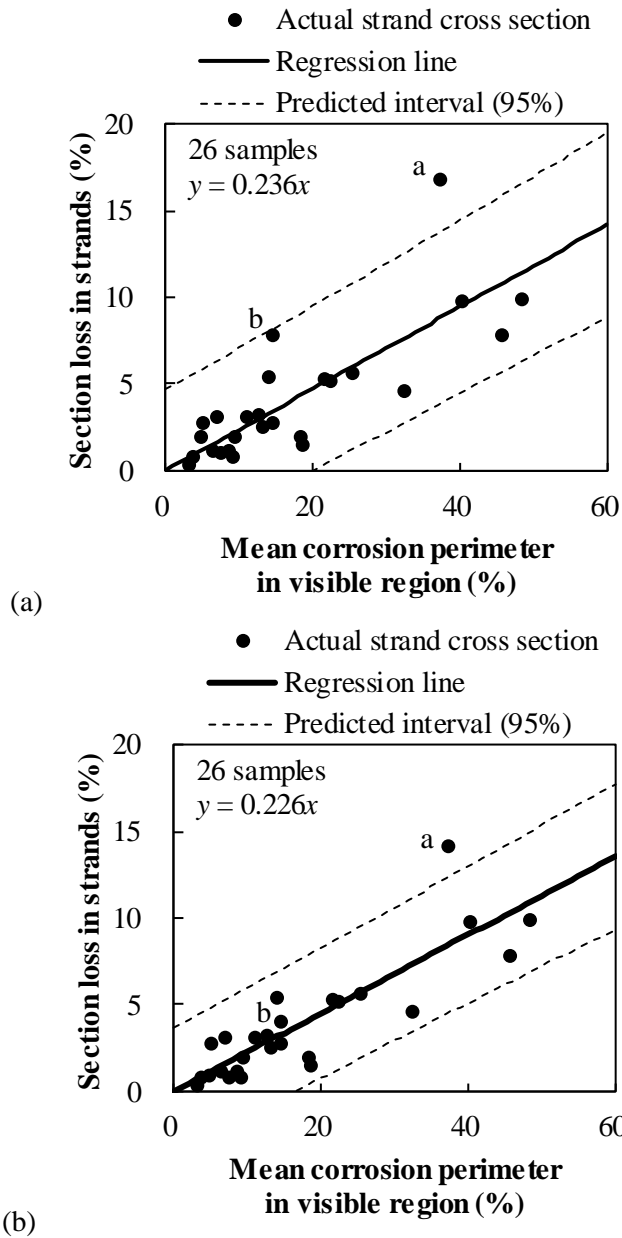


Fig. 5.8 Regression analysis for measured strand cross section with respect to mean corrosion perimeter: (a) considering all of wires; and (b) excluding wires which have an asymptomatic corrosion.

5.3 Application – Evaluating Remaining Strength of Corroded Strands

While the regression analysis for estimated section loss in strand was conducted in section 4.4, the regression analysis for generated corroded strands will be conducted in this section. Also, the residual strength of corroded strands are estimated by same procedure in section 4.4.

The results of regression analysis for generated corroded strands are presented in Fig. 5.6. The relationship between the remaining strength and the corrosion depth/perimeter is derived by substituting the regression line into Eq. (4.1) as formulated in Eqs. (5.8) and (5.9) and illustrated in Fig. 5.9.

$$\frac{F_{uc}}{F_{u0}} \times 100 = 100 - 1.39(0.405 p_s) = 100 - 0.563 p_s \quad (5.8)$$

$$\frac{F_{uc}}{F_{u0}} \times 100 = 100 - 1.39(0.171 L_s) = 100 - 0.238 L_s \quad (5.9)$$

The lower boundary of prediction interval in Fig. 5.9 can be formulated as:

$$\frac{F_{uc}}{F_{u0}} \times 100 = 100 - 1.39(0.405 p_s + 1.96 \sigma_s) = 97.1 - 0.563 p_s \quad (5.8)$$

$$\frac{F_{uc}}{F_{u0}} \times 100 = 100 - 1.39(0.171 L_s + 1.96 \sigma_s) = 96.0 - 0.238 L_s \quad (5.9)$$

As the remaining strength decreases to 5, 10, and 15%, the mean corrosion depth will be 3.7, 12.6, and 21.5% and the mean corrosion perimeter will be 4.2, 25.2, and 46.2%. The remaining strength of generated samples in terms of corrosion depth gives an conservative value than the results obtained from the estimated section loss in strand as shown in section 4.4.2. On the other hand, the remaining strength obtained from mean corrosion depth shows an opposite tendency.

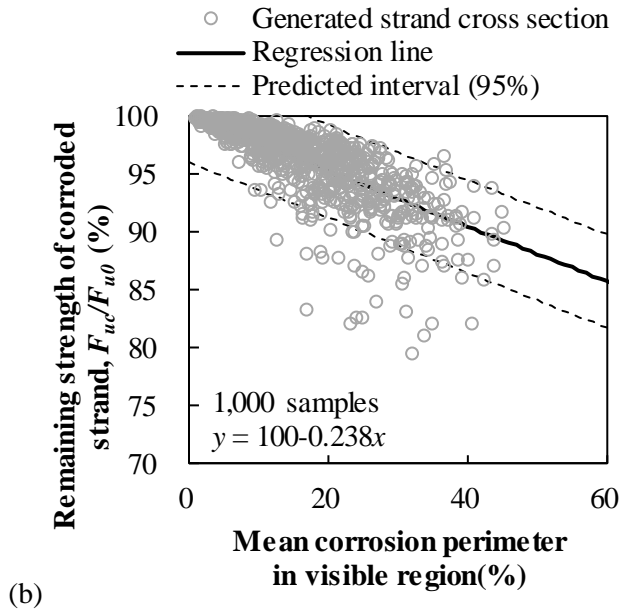
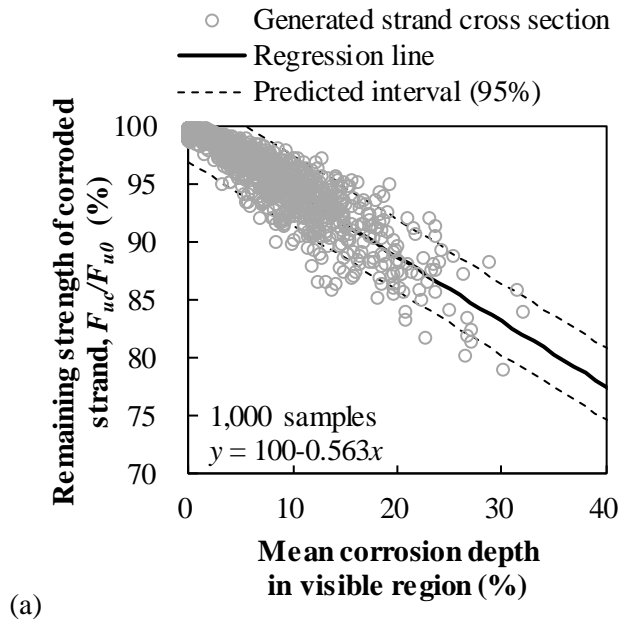


Fig. 5.9 Remaining strength of generated strands: (a) via mean corrosion depth; (b) via mean corrosion perimeter.

CHAPTER 6

Conclusions and Recommendations for Future Study

Estimating section loss in corroded prestressing tendons is essential for maintaining post-tensioned concrete bridges. If the section loss in a steel strand could be estimated from measurements such as corrosion depth or corrosion perimeter, it would help decision makers decide whether a tendon should be replaced or repaired.

Cross-sections of steel wires and strands corroded by infiltrating water with high chloride content were measured and analyzed. In this study, the parameters of corrosion depth and the corrosion perimeter aptly represented the section loss in both wire and strand. From the measurement results of corroded wires, it was found that the corrosion depth increased almost linear to increases in the section loss, whereas the corrosion perimeter rapidly increased until the section loss reached approximately 10%. The measurement results of strand is focused on the visible characteristics of corroded strands. The linearity between the visible characteristics and the section loss in strands are identified.

As an initial step for estimating section losses in corroded strands, corrosion models for steel wires were investigated. The existing corrosion models were evaluated using measurements, which showed that the existing models consistently underestimated the section losses for corrosion depth. The existing models could not be used to estimate losses for smaller sections due to an inability to simulate rapid increases in the corrosion perimeter of those sections. As a result, two corrosion models were proposed that assumed a convex shape for the corrosion surface.

These models successfully simulated corrosion progress in wires. The proposed models I and II used the corrosion depth and corrosion perimeter, respectively, to provide reliable estimates of section losses. Especially, the proposed model II conservatively estimates the section loss in wire for compensating the large dispersion of the corrosion perimeter. In addition, The proposed model III which utilized both the corrosion depth and corrosion perimeter proved their accuracy for estimating the section loss in wire.

The corrosion models are expanded to the strand level. Although it was not feasible to inspect the corrosion in invisible regions, a corrosion model for wires was successfully implemented to estimate the section losses in strands by individually estimating the section losses in wires and assembling them. Estimating section loss with respect to corrosion depth provided better accuracy compared with the use of corrosion perimeter. Estimating section loss of corroded strands using both corrosion depth and perimeter showed significantly smaller residual compared with estimating the section loss of corroded wires. Since the corrosion progress model for wires estimates the mean section loss with respect to corrosion depth and perimeters, estimates for the section losses of wires in visible regions compensated for the larger section losses in wires and improved the accuracy.

Implementing section loss estimation for evaluating the remaining strength of corroded strands showed that 95 and 90% of the remaining ultimate strengths of corroded strands could be limited by mean corrosion depths of about 6.9 and 17.1% or mean corrosion perimeters of about 2.2% and 16.2%, respectively. For practical purposes, the ultimate strength of the corroded strands with mean corrosion depths of 5 and 15% or mean corrosion depth of 2% and 15% could be 95 and 90%, respectively.

Monte Carlo simulation is adopted to manage the various combination of corroded strand. The probabilistic characteristics of corroded wires and strands are identified. Especially, the section loss in wire is modelled through GLM. The results of simulation are verified by comparison with the measured data.

The remaining strength is evaluated based on generated data. The evaluated remaining strength by the generated data show a smaller value than that by measured data because the correlation of corrosion between near wires is not considered during simulation process.

Although the proposed corrosion models were effective for estimating section losses based on measurements of corrosion depth and perimeter, the disparities that persist in the estimations of section loss due to the irregularities of corroded sections remains a problem, which should be carefully addressed in future studies. Moreover, it should be noted that the specimens were collected from corroded strands contaminated by water with high chloride content from the outside of a bridge. If the corrosion is caused by different sources, such as bleeding water or chloride mixed in cement grout, the corroded sections could differ from the results presented in this study.

The residual strength of collected strand samples is not measured value, but estimated value from the tensile test results of other strand samples in same bridge. If the ultimate strength of samples is tested, the section loss of tested samples would be problematic to be identified because necking occurs in the tested samples. The necking is a phenomenon of ductility of strand. Ductility of strand decreases as the corrosion degree of strand which means that the necking will decrease as severe corrosion degree of strand. Based on this fact, the fractured cross sections of strand after the tensile test should be carefully investigated for acquiring the section loss

in strand.

As mentioned earlier, the analyzed samples were collected from the limited corrosion environment. The chance to obtain a large quantity of corroded strands occurred from the operating bridge site is very limited. Therefore, the generation technique of corroded strands will be helpful in this case. Moreover, this generation technique needs to be advanced by integrating the update technique, which considers the corrosion environment, such as Bayesian update method for handling the various corrosion environments. At last, the section loss estimation procedure should expand to the entire tendon.

REFERENCES

AASHTO (2014). "LRFD Bridge Design Specifications." American Association of State Highway and Transportation Officials (AASHTO), Washington, D.C. ASTM. (1999). "Standard practice for preparing, cleaning and evaluating corrosion test specimens." G1-90, West Conshohocken, PA.

ASTM. (2005). "Standard guide for examination and evaluation of pitting corrosion." G46-94, West Conshohocken, PA.

Azizinamini, A., and Gull, J. (2012). "Improved Inspection Techniques for Steel Prestressing/Post-tensioning Strand: Volume I." Contract No. BDK80 977-13, Florida Department of Transportation, Tallahassee, FL.

Berg, K. M., and Schokker, A. J. (2012). "Development of Best Practices for Inspection of PT Bridges in Minnesota." MN/RC 2012-09, Minnesota Department of Transportation, Saint Paul, MN.

Berto, L., Vitaliani, R., Saelta, A., and Simioni, P. (2009). "Seismic assessment of existing RC structures affected by degradation phenomena." *Struct. Safety*, 31(4), 284-297.

Betti, R., West, A. C., Vermaas, G., and Cao, Y. (2005). "Corrosion and embrittlement in high-strength wires of suspension bridge cables." *J. Bridge Eng.*, 10.1061/(ASCE)1084-0702(2005)10:2(151), 151-162.

Cairns, J., Plizzari, G. A., Du, Y., Law, D. W., and Franzoni, C. (2005). "Mechanical properties of corrosion-damaged reinforcement." *ACI Mater. J.*, 102(4), 256-264.

Darmawan, M. S., and Stewart, M. G. (2007). "Spatial time-dependent reliabil-

ity analysis of corroding pretensioned prestressed concrete bridge girders." *Struct. Safety*, 29(1), 16-31.

Du, Y., Clark, L., and Chan, A. (2005). "Residual capacity of corroded reinforcing bars." *Mag. Concrete Res.*, 57(3), 135-147.

Eichinger, E. M., Diem, J., and Kollegger, J. "Assessment of Post-Tensioning Tendons in Vienna's Road Bridges." *Proc., IABSE Congress Rep., International Association for Bridge and Structural Engineering, Lucerne, Switzerland*, 1184-1191.

Faroz, S. A., Pujari, N. N., and Ghosh, S. (2016). "Reliability of a corroded RC beam based on Bayesian updating of the corrosion model." *Eng. Struct.*, 126, 457-468.

fib (International Federation for Structural Concrete). (2001). "Durability of Post-Tensioning Tendons : Technical report." *fib bulletin 15*, Lausanne, Switzerland.

Fox, J. (2015). *Applied regression analysis and generalized linear models*, Sage Publications.

Gonzalez, J., Andrade, C., Alonso, C., and Feliu, S. (1995). "Comparison of rates of general corrosion and maximum pitting penetration on concrete embedded steel reinforcement." *Cem. Concr. Res.*, 25(2), 257-264.

Guo, T., Sause, R., Frangopol, D. M., and Li, A. (2010). "Time-dependent reliability of PSC box-girder bridge considering creep, shrinkage, and corrosion." *J. Bridge Eng.*, 10.1061/(ASCE)BE.1943-5592.0000135, 29-43.

Hackl, J., and Kohler, J. (2016). "Reliability assessment of deteriorating reinforced concrete structures by representing the coupled effect of corrosion initiation and progression by Bayesian networks." *Struct. Safety*, 62(Supplement C), 12-23.

Hartt, W. H., and Lee, S. K. (2016). "Projecting Corrosion-Induced Bridge Tendon Failure Resulting from Deficient Grout: Part I—Model Development and Example Results." *Corrosion*, 72(8), 991-998.

Hartt, W. H., and Venugopalan, S. (2002). "Corrosion evaluation of post-tensioned tendons on the Mid Bay Bridge in Destin, Florida." Florida Department of Transportation, Tallahassee, FL.

Hattab, M. W. (2016). "A derivation of prediction intervals for gamma regression." *J. Stat. Comput. Sim.*, 86(17), 3512-3526.

James, G., Witten, D., Hastie, T., and Tibshirani, R. (2013). *An introduction to statistical learning*, Springer.

Jeon, C.-H., Lee, J.-B., and Shim, C.-S. (2017). "Tensile Test of Corroded Strand and Maintenance of Corroded Prestressed Concrete Girders." *World Academy of Science, Engineering and Technology, International Journal of Civil, Environmental, Structural, Construction and Architectural Engineering*, 11(10), 1363-1367.

Jones, L., Pessiki, S., Naito, C., and Hodgson, I. (2010). "Inspection Methods & Techniques to Determine Non Visible Corrosion of Prestressing Strands in Concrete Bridge Components: Task 2—Assessment of Candidate NDT Methods." ATLSS Report No. 09-09, Lehigh University, Bethlehem, PA.

Kashani, M. M., Crewe, A. J., and Alexander, N. A. (2013). "Use of a 3D optical measurement technique for stochastic corrosion pattern analysis of reinforcing bars subjected to accelerated corrosion." *Corros. Sci.*, 73, 208-221.

Kilduff, A. L., Moyer, K. L., McCool, G. E., Ahern, M. E., and Breen, J. E. (2013). "Corrosion Resistance Recommendations from Long-Term Exposure Testing of Post-Tensioning Systems." FHWA/TX-13/0-4562-5F, Texas Department of

Tarnsportation, Austin, Tx.

Kim, S., Frangopol, D. M., and Soliman, M. (2013). "Generalized probabilistic framework for optimum inspection and maintenance planning." *J. Struct. Eng.*, 10.1061/(ASCE)ST.1943-541X.0000676, 435-447.

KRTA (2016). "Korean Highway Bridge Design Code: General Bridge." Korea Road and Transportation Association (KRTA),, Seoul, KR.

Lee, B.-Y., Koh, K., Ismail, M., Ryu, H., and Kwon, S. (2017). "Corrosion and Strength Behaviors in Prestressed Tendon under Various Tensile Stress and Impressed Current Conditions." *Adv. Mater. Sci. Eng.*, 2017, 1-7.

Li, F., Luo, X., Wang, K., and Ji, Y. (2017). "Pitting Damage Characteristics on Prestressing Steel Strands by Combined Action of Fatigue Load and Chloride Corrosion." *J. Bridge Eng.*, 10.1061/(ASCE)BE.1943-5592.0001057, 04017023.

Li, S., Xu, Y., Li, H., and Guan, X. (2014). "Uniform and pitting corrosion modeling for high-strength bridge wires." *J. Bridge Eng.*, 10.1061/(ASCE)BE.1943-5592.0000598, 04014025.

Ma, Y., Zhang, J., Wang, L., and Liu, Y. (2013). "Probabilistic prediction with Bayesian updating for strength degradation of RC bridge beams." *Struct. Safety*, 44, 102-109.

Nakagawa, Y., and Mikami, T. (2010). "Investigation of the main girder in the Omi bridge repair status report." *Prevention of Disasters: No. 23*, Ministry of Land, Infrastructure, Transport and Tourism Kinki Regional Development and Bureau, Kobe, Japan (in Japanese).

Nakamura, S., and Suzumura, K. (2012). "Experimental study on fatigue strength of corroded bridge wires." *J. Bridge Eng.*, 10.1061/(ASCE)BE.1943-5592.0000366, 200-209.

Nelder, J. A., and Wedderburn, R. W. M. (1972). "Generalized linear models." *J. R. Stat. Soc. Ser. A-G.*, 135(3), 370-384.

Permeh, S., Vigneshwaran, K., and Lau, K. (2016). "Corrosion of Post-Tensioned Tendons with Deficient Grout." Contract No. BDV29-977-04, Florida Department of Transportation, Tallahassee, FL.

Poston, R. W., and Wouters, J. P. (1998). "Durability of Precast Segmental Bridges: Final Report." NCHRP Web Document No. 15, Project 20-7/Task 92, National Cooperative Highway Research Program (NCHRP), Washington, DC.

Provan, J., and Rodriguez III, E. J. C. (1989). "Part I: Development of a Markov description of pitting corrosion." 45(3), 178-192.

PTI, and American Segmental Bridge Institute (ASBI) (2012). Guide specification for grouted post-tensioning, Post-Tensioning Institute (PTI), Farmington Hills, MI.

Reis, R. A. (2007). "Corrosion Evaluation and Tensile Results of Selected Post-Tensioning Strands at the SFOBB Skyway Seismic Replacement Project Phase III Report." California Department of Transportation, Sacramento, CA.

Sason, A. S. (1992). "Evaluation of degree of rusting on prestressed concrete strand." *PCI J.*, 37(3), 25-30.

Sheikh, A., Boah, J., and Hansen, D. (1990). "Statistical modeling of pitting corrosion and pipeline reliability." *Corrosion*, 46(3), 190-197.

Shibata, T. (1991). "Evaluation of corrosion failure by extreme value statistics." *ISIJ Int.*, 31(2), 115-121.

SMFMC (2017). "Synthesis Report : Academic service contract related with Maintenance of PSC box girder bridges in Seoul jurisdiction." Seoul Metropolitan Facilities Management Corporation (SMFMC), Seoul, Korea (in Korean).

Stewart, M. G. (2004). "Spatial variability of pitting corrosion and its influence on structural fragility and reliability of RC beams in flexure." *Struct. Safety*, 26(4), 453-470.

Stewart, M. G. (2009). "Mechanical behaviour of pitting corrosion of flexural and shear reinforcement and its effect on structural reliability of corroding RC beams." *Struct. safety*, 31(1), 19-30.

Stewart, M. G., and Rosowsky, D. V. (1998). "Time-dependent reliability of deteriorating reinforced concrete bridge decks." *Struct. Safety*, 20(1), 91-109.

Torres-Acosta, A. A., and Martinez-Madrid, M. (2003). "Residual life of corroding reinforced concrete structures in marine environment." *J. Mater. Civ. Eng.*, 10.1061/(ASCE)0899-1561(2003)15:4(344), 344-353.

Trejo, D., Hueste, M. B. D., Gardoni, P., Pillai, R. G., Reinschmidt, K. F., Im, S. B., Kataria, S., Hurlebaus, S., Gamble, M., and Ngo, T. T. (2009). "Effect of Voids in Grouted, Post-Tensioned Concrete Bridge Construction: Volume 1—Electrochemical Testing and Reliability Assessment." FHWA/TX-09/0-4588-1 Vol. 1, Texas Department of Transportation, Austin, TX.

Tuutti, K. (1982). "Corrosion of steel in concrete." Ph.D. thesis, Swedish Cement and Concrete Research Institute, Stockholm, Sweden.

Val, D. V., and Melchers, R. E. (1997). "Reliability of deteriorating RC slab bridges." *J. Struct. Eng.*, 10.1061/(ASCE)0733-9445(1997)123:12(1638), 1638-1644.

Wu, X., and Li, H. "Effect of strain level on corrosion of prestressing steel strands." *Proc., IABSE Symposium Rep., International Association for Bridge and Structural Engineering*, 292-299.

초 록

유철환

건설환경공학부

서울대학교 대학원

긴장재에 부식이 발생할 경우, 부식이 발생한 긴장재의 교체나 보수를 통해 긴장재를 유지관리해야 한다. 효율적인 유지관리를 위해선 긴장재의 단면손실을 바탕으로 교체나 보수의 결정이 내려져야 한다. 그러나 현재 가용한 긴장재 조사 방법으로는 긴장재의 단면손실에 대한 정성적인 평가만 가능하며, 정량적으로 평가하지는 못하는 상황이다. 이런 이유로 긴장재의 단면손실을 정량적으로 추정할 수 있는 방법을 제안하고자 하였다.

실제 교량의 부식 환경을 파악하기 위해 염화물과 수분의 침투로 인해 부식이 발생했던 교량 현장의 강연선을 수집하였다. 수집한 강연선의 단면손실을 알기 위해 접사렌즈를 부착한 카메라를 이용하여 소선과 강연선의 접사 사진을 촬영하였으며, 촬영한 사진을 바탕으로 소선과 강연선 단위의 부식 특성을 파악하였다. 우선, 소선의 부식깊이, 부식둘레, 단면손실을 파악하였으며, 이후 강연선의 관찰가능영역과 관찰불가능영역을 구분하여 관찰가능한 강연선의 부식깊이, 부식둘레, 부식소선 개수 등을 파악하였다. 소선 단위의 분석을 통해, 소선의 부식깊이, 부식둘레가 단면손실과 연관성을 가지며 부식 진행 초기에는 부식둘레의 진행 속도

가 부식깊이에 비해 빠르다는 것을 확인하였다. 강연선 단위의 분석을 통해 관찰가능한 부식깊이, 부식둘레가 강연선의 단면손실과 상관성을 나타내는 것을 확인하였다. 또한, 관찰가능한 부식소선의 개수가 강연선의 대략적인 단면손실을 알 수 있는 지표가 될 수 있음을 보였다.

소선에서 측정한 지표를 이용하여 소선의 단면손실을 추정하기 위해 소선의 부식 진행을 반영한 부식 모델을 제안하였다. 측정결과를 바탕으로 기존의 부식 모델은 부식깊이에 따른 소선의 단면손실을 과소평가한다는 점을 밝혀내었다. 실제 단면의 경우 부식깊이에 비해 부식둘레로의 부식 확산이 빠르기 때문에 볼록한 형상의 부식 모델을 제안하였다. 또한, 제안한 부식 모델이 실제 단면손실을 보다 정확하게 맞춘다는 점을 확인하여 제안 모델의 효율성을 입증하였다.

소선에 대해 제안한 부식 모델과 관찰가능한 부식깊이/부식둘레를 사용하여 강연선의 단면손실을 추정하는 방법을 제안하였다. 강연선의 단면손실 추정 결과는 부식깊이와 부식둘레의 특성에 따라 오차의 발생 양상에서 차이를 보였다. 이 오차로 볼 때, 부식깊이를 사용하여 추정하는 것이 부식둘레를 사용하여 추정하는 것보다 정확한 결과를 제공한다고 할 수 있다. 추정한 단면손실을 적용하여 부식 강연선의 잔여 강도를 평가하였다. 평가 결과, 강연선의 평균부식깊이가 5%, 15%에 도달할 때 강연선의 극한강도가 5%, , 10% 감소하였다.

강연선의 다양한 부식을 고려하여 관찰가능지표와 강연선의 단면손실 간 상관관계를 규정하고자 몬테 카를로 시뮬레이션을 수행하였다. 이를 위해 강연선 부식에 포함된 확률특성들을 정의하고 확률모델을 구성

하였다. 시뮬레이션으로 생성된 부식 강연선은 측정된 결과와 비슷한 양상을 보였다. 생성결과를 바탕으로 한 강연선의 단면손실 추정 방법을 제안하였다.

주요어: 부식, 강연선, 소선, 외부긴장재